



HAL
open science

Fractal Distribution of Subduction-Related Crack-Seal Veins (Schistes Lustrés, W. Alps): Implications for Fluid Flow and Rupture Processes at the Downtip End of the Seismogenic Zone

Clément Herviou, Philippe Agard, Anne Verlaguet, Thomas Gyomlai,
Guillaume Bonnet, Kevin Mendes, Alexis Plunder

► To cite this version:

Clément Herviou, Philippe Agard, Anne Verlaguet, Thomas Gyomlai, Guillaume Bonnet, et al.. Fractal Distribution of Subduction-Related Crack-Seal Veins (Schistes Lustrés, W. Alps): Implications for Fluid Flow and Rupture Processes at the Downtip End of the Seismogenic Zone. *Journal of Geophysical Research: Solid Earth*, 2023, 128 (10), 10.1029/2022JB026317 . hal-04287339

HAL Id: hal-04287339

<https://brgm.hal.science/hal-04287339v1>

Submitted on 15 Nov 2023

HAL is a multi-disciplinary open access archive for the deposit and dissemination of scientific research documents, whether they are published or not. The documents may come from teaching and research institutions in France or abroad, or from public or private research centers.

L'archive ouverte pluridisciplinaire **HAL**, est destinée au dépôt et à la diffusion de documents scientifiques de niveau recherche, publiés ou non, émanant des établissements d'enseignement et de recherche français ou étrangers, des laboratoires publics ou privés.

JGR Solid Earth

RESEARCH ARTICLE

10.1029/2022JB026317

Key Points:

- Lawsonite- and Fe-Mg carpholite-bearing crack-seal veins formed during subduction, at the depth of the slow slip and tremor region
- Vein thicknesses, spacings and clustering suggest a pervasive fluid flow during subduction, in agreement with geochemical studies
- The distribution of crack-seal inclusions in the veins fits slow slip and tremor features suggesting a likely record of these events

Supporting Information:

Supporting Information may be found in the online version of this article.

Correspondence to:

C. Herviou,
clement.herviou@univ-lyon1.fr

Citation:

Herviou, C., Agard, P., Verlaquet, A., Gyomlai, T., Bonnet, G., Mendes, K., & Plunder, A. (2023). Fractal distribution of subduction-related crack-seal veins (Schistes Lustrés, W. Alps): Implications for fluid flow and rupture processes at the downdip end of the seismogenic zone. *Journal of Geophysical Research: Solid Earth*, 128, e2022JB026317. <https://doi.org/10.1029/2022JB026317>

Received 4 JAN 2023

Accepted 2 OCT 2023

Author Contributions:

Conceptualization: Clément Herviou, Philippe Agard

Investigation: Clément Herviou, Philippe Agard, Kevin Mendes, Alexis Plunder

Methodology: Clément Herviou, Philippe Agard, Thomas Gyomlai, Guillaume Bonnet







Visualization: Clément Herviou

Writing – original draft: Clément Herviou

Writing – review & editing: Clément Herviou, Philippe Agard, Anne Verlaquet, Thomas Gyomlai, Guillaume Bonnet, Kevin Mendes, Alexis Plunder

© 2023. American Geophysical Union.
All Rights Reserved.

Fractal Distribution of Subduction-Related Crack-Seal Veins (Schistes Lustrés, W. Alps): Implications for Fluid Flow and Rupture Processes at the Downdip End of the Seismogenic Zone

Clément Herviou^{1,2} , Philippe Agard¹, Anne Verlaquet¹ , Thomas Gyomlai¹ , Guillaume Bonnet^{1,3} , Kevin Mendes¹ , and Alexis Plunder⁴ 

¹Institut des Sciences de la Terre de Paris, CNRS-INSU, Sorbonne Université, Paris, France, ²Department of Earth, Marine and Environmental Sciences, University of North Carolina, Chapel Hill, NC, USA, ³Institute of Geological Sciences, University of Bern, Bern, Switzerland, ⁴BRGM, Orléans, France

Abstract In the Western Alps, oceanic lithosphere fragments recovered from subduction are exposed continuously across the Liguro-Piemont domain. In this nappe-stack, the Schistes Lustrés metasediments are volumetrically dominant and contain large amounts of high-pressure lawsonite- and Fe-Mg carpholite-bearing veins. These veins formed close to peak burial conditions at 30–60 km depth where deep slow slips and tremors occur. In the 12 studied outcrops, vein thickness distribution fit power laws while vein spacings and clustering show significant deviations from power laws, interpreted as the result of truncation artifacts and, possibly, at least in part, of later ductile deformation. Vein distribution at the outcrop scale suggests that fluids mostly circulated pervasively through the rock rather than along major localized conduits, in agreement with geochemical studies. Through the study of vein textures at macroscopic and microscopic scales, we showed that these high-pressure veins formed by an incremental crack-seal mechanism under tensile and shear failure and possibly between extremely weak planes. The spacings between crack-seal inclusion trails and bands, which is in the same order as slip increments for low frequency-earthquakes, fit a power law for a small fractal range with a fractal exponent similar to those estimated for slow slip events and ordinary earthquakes. In addition, the shear stress drop estimated for these veins is consistent with those inferred for slow slips and tremors. Data suggest that these veins, formed at the downdip end of the seismogenic zone, may correspond to the record of successive low-frequency earthquakes during subduction of the Liguro-Piemont ocean.

Plain Language Summary Modern subduction zones—places where a tectonic plate sinks under another—host a zone at ~25–55 km depth, where anomalous seismic velocities and atypical earthquakes suggest the presence of fluids. In this manuscript, we study a fossil subduction zone preserved in the Western Alps where rocks were buried at the same depth range. The occurrence of metamorphic veins (mineralized fractures) witnesses the fossil fluid circulation and fluid-rock interactions. Their statistical distributions suggest that fluid flow was pervasive in the rocks, rather than localized in major conduits. The textures of these veins show their formation by successive fracturing events. The distribution of cracking increments fits features of the seismic events classically described at these depths (the slow slips and tremors). These veins are therefore considered to be a likely record of these slow earthquakes during subduction.

1. Introduction

A major mechanical transition along the plate interface lies immediately downdip of the seismogenic zone, struck by subduction megathrust earthquakes (e.g., Agard et al., 2018; Lay et al., 2012; Peacock & Hyndman, 1999; Figure 1a). In this region, most subduction zones exhibit a few kilometer-thick low-velocity seismic layer characterized by high Poisson's and V_p/V_s ratios, consistent with near-lithostatic pore fluid pressure (e.g., Audet & Bürgmann, 2014; Audet et al., 2009; Bostock, 2013; Peacock et al., 2011; Figure 1a). This horizon is generally thought to originate from the presence of mafic crust and/or underplated sediments (Abers et al., 2009; Behr & Bürgmann, 2021; Bostock, 2013; Calvert et al., 2011; Delph et al., 2018, 2021; Hansen et al., 2012; Paulatto et al., 2017; Tewksbury-Christle & Behr, 2021). A wide array of seismic events, including transient slow slip events, low- and very-low-frequency earthquakes and episodic tremor and slip events (Dragert et al., 2001; Obara, 2002; Obara & Kato, 2016; Rogers & Dragert, 2003), referred to as deep slow slips and tremors (SST;

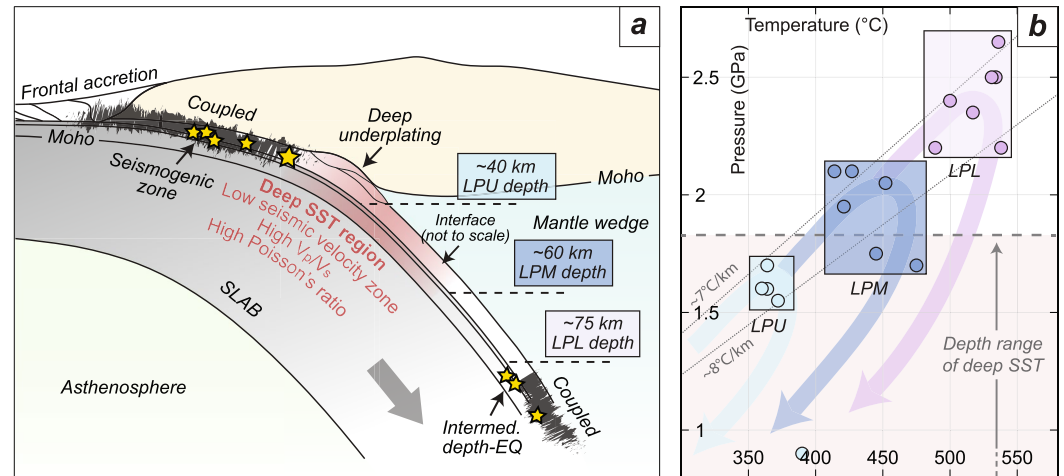


Figure 1. (a) Major mechanical transitions in subduction zones and approximate peak burial depths of Liguro-Piemont units. (b) Pressure-Temperature (P-T) conditions of Liguro-Piemont units after Herviou et al. (2022) and depth range of deep slow slips and tremors after Behr & Bürgmann (2021). Each circle corresponds to the mean P-T conditions estimated for independent tectonic slices. LPU: Liguro-Piemont Upper units; LPM: Liguro-Piemont Middle units; LPL: Liguro-Piemont Lower units; SST: slow slips and tremors; EQ: earthquakes.

Behr & Bürgmann, 2021), typifies this region at depths and temperatures of about 25–55 km and 350–550°C (Figures 1a and 1b; e.g., see also Condit et al., 2020; Peacock, 2009).

Although the role of fluids is generally invoked in the nucleation and recurrence of SST (Audet & Bürgmann, 2014; Obara, 2002; Saffer & Tobin, 2011), the preserved rock-record of these events in exhumed subduction complexes remains highly debated (Behr & Bürgmann, 2021; Kirkpatrick et al., 2021; Oncken et al., 2021; see also Hoover et al., 2022). While shear and dilatant crack-seal veins reflecting episodic fracturing, fluid infiltration and mineral growth events are regularly invoked as a rock record of SST and/or earthquakes in exhumed subduction sediments (Cerchiari et al., 2020; Condit & French, 2022; Fagereng & Harris, 2014; Fagereng et al., 2011; Fisher & Brantley, 1992, 2014; Fisher et al., 1995; Giuntoli & Viola, 2021, 2022; Muñoz-Montecinos et al., 2020; Raimbourg et al., 2021; Ujiie et al., 2018; Vannucchi et al., 2010), only few studies have so far provided quantitative statistical support on the link between crack-seal veins and SST.

By measuring the spacings between crack-seal inclusion bands (generally a few micrometers), interpreted as one increment of displacement, and the length of individual slip surfaces in the field, Fagereng et al. (2011) obtained potential stress drop estimates of ~30 kPa for the Chrystalls Beach complex (New Zealand), similar to those characterizing low-frequency earthquakes. For quartz-bearing crack-seal veins of the Makimine mélange (Shimanto Belt, Japan), Ujiie et al. (2018) inferred a multi-year healing time, compatible with the recurrence intervals of SST, using the spacings of inclusion bands and a kinetic model of quartz precipitation. In these veins, the changes in band spacings are thought to reflect the temporal change in the recurrence intervals of SST during megathrust earthquake cycles (Nishiyama et al., 2021). Fisher et al. (1995) and Fisher and Brantley (2014), for en-échelon quartz veins of the Kodiak complex, calculated that salty fluids (7.5 wt.% NaCl eq.) can seal few microns-wide fractures at the scale of a week, compatible with the duration of slow earthquakes. Finally, the characteristic range of inclusion bands spacings in crack-seal veins from several subduction complexes (Chrystalls Beach complex; Makimine mélange; Franciscan complex, USA; Livingston fault, New Zealand) led Williams and Kirkpatrick (2022) to propose a slip-limited model (constant slip increments, exponential distribution of the rupture area) for the low-frequency earthquakes.

These studies concern temperatures fitting those considered for the downdip end of the seismogenic zone, however pressure estimates suggest subduction depths (~10–15 km depth, Figure 1a; ~300°C – <0.55 GPa for the Chrystall Beach complex; 300–350°C – 0.3–0.5 GPa for the Makimine mélange; 270°C – 0.22–0.3 GPa for the Kodiak complex; Brantley et al., 1997; Fagereng & Cooper, 2010; Palazzin et al., 2016; Toriumi & Teruya, 1988) shallower than the deep SST region (25–55 km, Behr & Bürgmann, 2021; and possibly down to 60–70 km depth, Brown et al., 2013). The description and statistical measurement of metamorphic veins

therefore require further investigation to decipher the mechanisms of fluid transfer in the deep SST region, and to assess the potential relationships between the rock record and seismic processes.

Remnants of a subducted slow-spreading ocean (Lagabrielle & Cannat, 1990) are exposed in the Liguro-Piemont domain of the Western Alps (Agard, 2021; Agard & Handy, 2021; Deville et al., 1992; Herviou et al., 2022), which provides an access to subduction processes from ~30 to 80 km depths (Agard, 2021; Agard et al., 2002, 2018; Bebout et al., 2013; Berger & Bousquet, 2008; Herviou et al., 2021, 2022; Figures 1a and 1b). Distinct subduction slices were recognized in the Western Alps, with a trimodal depth distribution (35–45 km, 55–65 km and 70–80 km; Herviou et al., 2022; Figures 1a, 1b, 2a, and 2b) marked by an increase in metamorphic conditions from the Upper (LPU; 320–400°C – 1.2–1.9 GPa) to the Middle (LPM; 415–475°C – 1.7–2.2 GPa) and to the Lower units (LPL; 500–580°C – 2.2–2.8 GPa). The metasedimentary fraction, known as the Schistes Lustrés (e.g., Agard et al., 2001) dominates in the blueschist-facies LPU and LPM units (>90%), whereas the eclogite-facies units (LPL) are richer in mafic-ultramafic rocks (>40%; Herviou et al., 2022). The similarity between the peak burial depths of the LPU, LPM, and LPL units and those inferred for tectonic slicing and underplating, in both modern and fossil subduction zones, points to specific mechanisms controlling transient changes in interplate coupling at these depths (Agard et al., 2018; Cubas et al., 2022; Herviou et al., 2022; Plunder et al., 2015).

In the LPU and LPM blueschist-facies units, which were sliced from the downgoing plate at depths similar to those considered as the locus of deep SST (Behr & Bürgmann, 2021; Figures 1a and 1b), there are abundant metamorphic veins hosting water-rich high-pressure low-temperature (HP-LT) minerals such as lawsonite and Fe-Mg carpholite (Agard et al., 2000, 2001; Herviou et al., 2021; Lefeuvre et al., 2020), thereby highlighting fluid transfer at the base of the seismogenic zone. In order to clarify and quantify the relationships between the rock record and processes occurring at the subduction plate interface, this work reports measurements of vein thicknesses, vein spacings, vein clustering and crack-seal band spacings, as well as their respective statistical distributions, across 12 outcrops of the LPU and LPM units.

2. Distribution of Hydrothermal/Metamorphic Veins in Rocks

Hydrothermal/metamorphic veins reflecting crystal growth in cracks are almost ubiquitous in rocks and are considered as the best record of fluid circulation and fluid-rock interaction at depth (e.g., Fisher et al., 1995; Verlaquet et al., 2011; Widmer & Thompson, 2001). Most of these cracks are interpreted to form by tensile or shear brittle failure of the rocks under high fluid pressures and/or changes in the magnitude or orientation of stresses (Bons et al., 2012; Oliver & Bons, 2001).

Characterization of fluid sources and fluid pathways in rocks is central in the study of veins (e.g., Herviou et al., 2021; Hoover et al., 2023; Locatelli et al., 2019; Muñoz-Montecinos et al., 2021; Rajic et al., 2023; Spandler et al., 2011). Geochemical tracers, as fluid inclusions, trace elements and isotopes are generally used to provide clues on fluid compositions and sources (Roedder, 1984; Spandler & Pirard, 2013; Valley, 1986). Vein mineralization and microtextures inform about mineral precipitation and fluid supply mechanisms in veins, either by dominant local diffusive transport or larger scale advective transport (Bons et al., 2012; Oliver & Bons, 2001). Fluid flow patterns and distances over which fluids migrate are largely controlled by the material viscosity and the porosity-dependent dynamic permeability (Yarushina & Podladchikov, 2015). Since the opening of cracks creates transient permeability changes amenable to fluid circulation, the study of vein thicknesses, vein spacings and their clustering in rocks sheds light on how the fluids pervade the rocks or localize in interconnected networks along major zones of weakness.

The statistical analysis of veins from various geological settings has shown that vein thicknesses generally follow power-law distributions, where the number of objects $N(a)$ of size a or larger satisfies the relationship $N(a) \propto a^{-D}$ (D being the fractal dimension; André-Mayer & Sausse, 2007; Clark et al., 1995; Fagereng, 2011; Fisher et al., 1995; Gillespie et al., 1999; Lahiri et al., 2020; Mazzarini et al., 2011; McCaffrey & Johnston, 1996; McCaffrey et al., 1993; Monecke et al., 2001; Roberts et al., 1999; Sanderson et al., 2008, 1994). Fractal theory and scale-invariant laws help linking small scale observations to large scale processes (Allègre et al., 1982; Mandelbrot, 1982; Pickering et al., 1995; Turcotte, 1986, 1989) and a wide variety of geological features have been identified as being well described by fractals such as the distribution of fracture spacing and apertures (Barton & Zoback, 1992; Hooker et al., 2013; La Pointe, 1988; Ledésert et al., 1993; Velde et al., 1990, 1991) and of fragmented material (Blenkinsop, 1991; Blenkinsop & Fernandes, 2000), as well as the scaling of

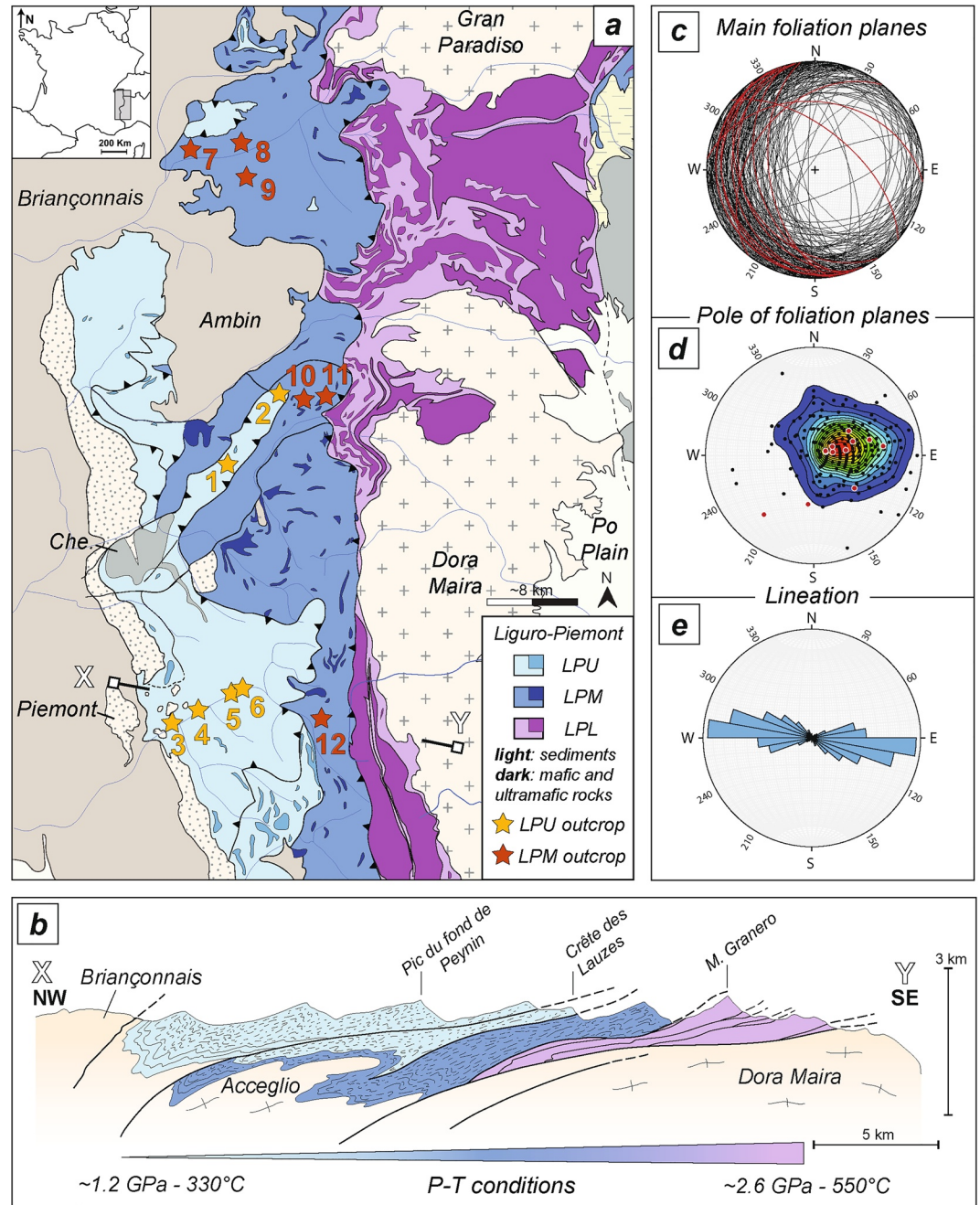


Figure 2. Geological setting of the Liguro-Piemont domain. (a) Structural map of the Western Alps with focus on the Liguro-Piemont domain showing the distribution of the three types of units throughout the complex and the location of the studied outcrops. Modified after Herviou et al. (2022). (b) Schematic cross-section along the studied area highlighting the stacking of the Liguro-Piemont units and the eastward increase in metamorphic grade. Modified after Lagabriele (1987) and Herviou et al. (2022). (c-e) Main foliation planes, poles and lineations plotted on Schmidt net lower hemisphere. Red planes and poles in (c) and (d) correspond to the studied outcrops. LPU: Liguro-Piemont Upper units; LPM: Liguro-Piemont Middle units; LPL: Liguro-Piemont Lower units; Che.: Chenaillet massif.

faults and earthquakes (Gutenberg & Richter, 1954; Jackson & Sanderson, 1992; Pickering et al., 1995, 1996; Watterson, 1986).

The vein length-thickness ratio (Johnston & McCaffrey, 1996; McCaffrey et al., 1993; Stowell et al., 1999), as well as the vein clustering across outcrops (Barton, 1995; Fagereng, 2011; Holland & Urai, 2010; Magde et al., 1995;

Manning, 1994), are also best described by power-law distributions. In contrast, vein spacings either follow power-law (Fagereng, 2011; Fisher et al., 1995; Mazzarini et al., 2011) or log-normal/negative exponential distributions (André-Mayer & Sausse, 2007; Fisher et al., 1995; Gillespie et al., 1999; Johnston & McCaffrey, 1996; McCaffrey & Johnston, 1996; McCaffrey et al., 1993; Sanderson et al., 2008; Simpson, 2000).

Most of these studies are based on extension veins, for which D values allow estimating if the total extension was dominantly accommodated by growth in larger veins or opening of thinner veins (e.g., Fagereng, 2011). Using stochastic models, Clark et al. (1995) showed that a power-law distribution of extension vein thicknesses can be produced by incremental growth of existing veins and limited initiation of new fractures. Estimating the proportion of thick versus thin veins also informs on strain localization and fluid transfer. Vein spacing distribution, as vein clustering, is considered to derive from the initial spacing of fractures and their D values also give clues on how the fluids pervaded the rocks or localized in specific zones (Manning, 1994; Simpson, 2000).

Most published works, however, have dealt with veins from mineralized ore deposits (André-Mayer & Sausse, 2007; Barton, 1995; Foxford et al., 2000; Gillespie et al., 1999; Johnston & McCaffrey, 1996; Lahiri et al., 2020; McCaffrey & Johnston, 1996; McCaffrey et al., 1993; Monecke et al., 2001; Roberts et al., 1999; Sanderson et al., 1994, 2008) or low-grade metamorphic rocks (Clark et al., 1995; Fagereng, 2011; Fisher et al., 1995; Holland & Urai, 2010; Simpson, 2000; Stowell et al., 1999). None has reported the statistical distribution of HP-LT metamorphic veins despite their large amounts in subduction complexes (Agard et al., 2000; Herviou et al., 2021; Muñoz-Montecinos et al., 2020, 2023), where the successive dehydration reactions accompanying burial of the downgoing plate (Schmidt & Poli, 2014), associated to the low porosity/permeability of rocks (Ganzhorn et al., 2019), likely generate large fluid pressure variations as expected for the SST environment (e.g., Behr & Bürgmann, 2021).

3. Geological Setting

Remnants of the Liguro-Piemont slow-spreading oceanic domain subducted below Adria/Apulia are found in the Western Alps (Agard, 2021; Agard & Handy, 2021; Deville et al., 1992). These rocks were buried between ~30 and 80 km depth (Agard et al., 2001, 2002, 2009; Herviou et al., 2022) and form a HP-LT nappe-stack known as the Liguro-Piemont domain (e.g., Agard, 2021) or the Schistes Lustrés complex (owing to their characteristic sediments; Agard et al., 2001; Caron, 1977; Deville et al., 1992; Tricart & Schwartz, 2006). After peak burial between ~60 and ~40 Ma, these rocks were scrapped off as tectonic slices from the downgoing plate, and exhumed from the Late Eocene to the Miocene (Agard et al., 2002; Angiboust & Glodny, 2020; Gyomlai et al., 2023; Herviou & Bonnet, 2023; Schwartz et al., 2007, 2020).

Several units corresponding to independent subduction slices were identified across the complex (Fudral, 1996; Lagabriele, 1987). Herviou et al. (2022) demonstrated the existence of a trimodal distribution of the units, with an almost continuous eastward increase in peak burial conditions from the Upper units (LPU; 320–400°C – 1.2–1.9 GPa) to the Middle units (LPM; 415–475°C – 1.7–2.2 GPa) and to the Lower units (LPL; 500–580°C – 2.2–2.8 GPa; Figures 1b, 2a, and 2b). The LPU and LPM blueschist-facies units are dominated by sediments (>90%; Schistes Lustrés s.s.; Figure 2a), whereas the eclogite-facies LPL units are much richer in mafic-ultramafic rocks (>40%; Figure 2a).

Successive episodes of deformation were described and dated in the Schistes Lustrés complex of the Cottian Alps (Agard et al., 2001, 2002; Figures 2c–2e and 3a–3h): the first stage (D1) corresponds to an early foliation, associated to the development of EW trending folds and the crystallization of peak metamorphic assemblages at ~62–55 Ma. The second fabric (D2) dated at ~51–45 Ma corresponds to the ductile east-vergent deformation accompanying early exhumation under blueschist-facies conditions. The third episode (D3), dated at ~38–35 Ma, is marked by top-to-the-west ductile to brittle deformation and is related to the exhumation in greenschist-facies conditions. This phase coincides with the ductile exhumation of large mafic-ultramafic complexes such as the Monviso massif (Angiboust & Glodny, 2020). Finally, two late fabrics (D4 and D5; Tricart & Schwartz, 2006), corresponding to small-scale boudinage and west-dipping normal faulting, characterize the ductile-brittle transition during late exhumation. All these tectonic patterns resulted in a flat to gently west-dipping foliation (S1–S2) mostly formed by D1–D2 patterns with stretching lineations trending N090 to N110 on average (Figures 2c–2e and 3a–3h).

Metamorphic veins are ubiquitous in the Schistes Lustrés LPU and LPM blueschist-facies metasediments. Some contain diagnostic HP-LT minerals (as described in detail below): (a) lawsonite-bearing veins (Figures 3a, 3c,

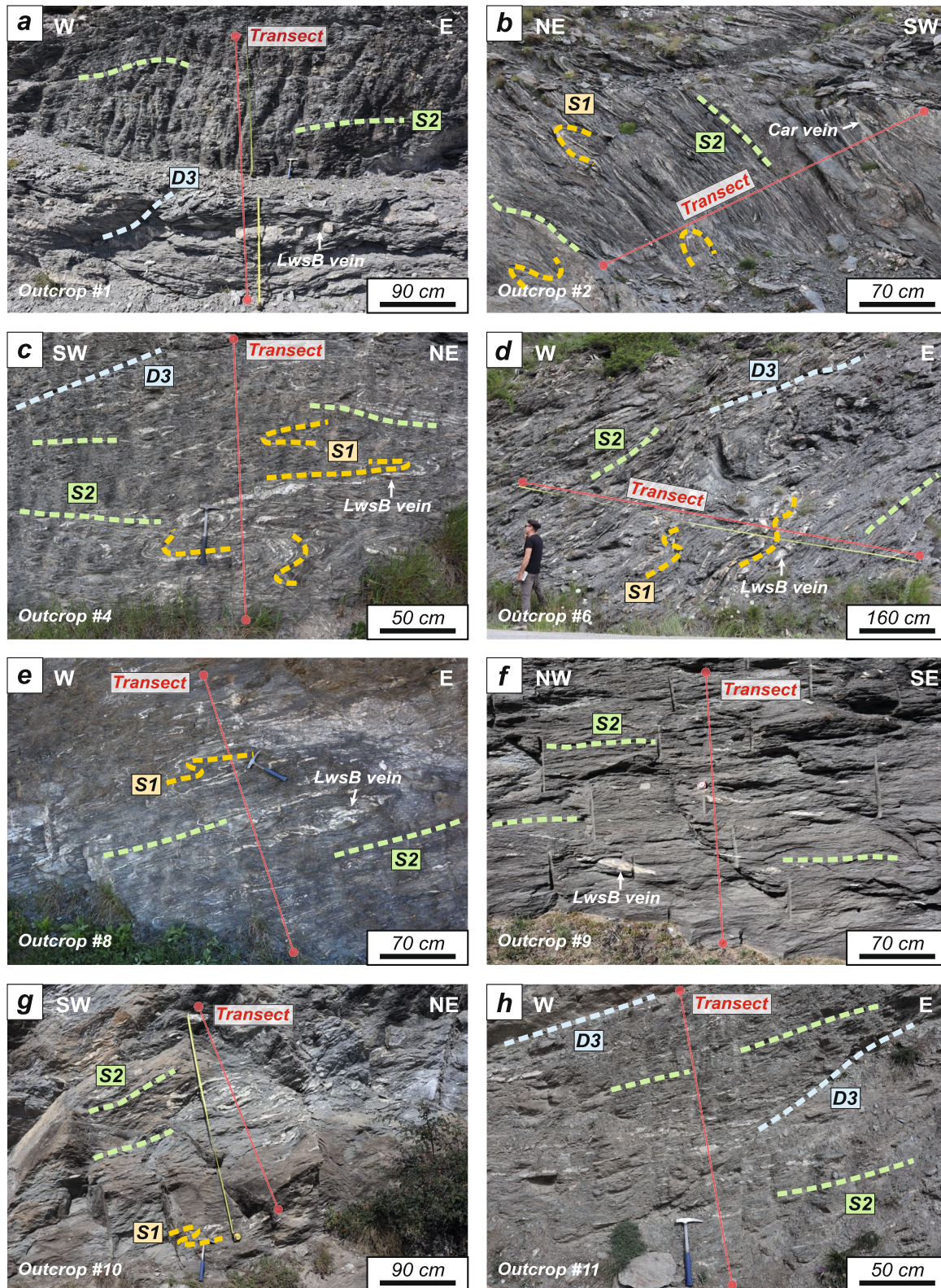


Figure 3. (a–h) Schistes Lustrés outcrops with deformation stages, metamorphic veins and studied transects. The different stages (D1–D3) lead to the development of a main S1–S2 foliation intersected by later D3 shear bands. Most of the veins are folded in the S1–S2 foliation and attributed to the earliest deformation stage (D1). Car: Fe–Mg carpholite; Lws: lawsonite.

Table 1
Studied Outcrops, Corresponding Localities, Estimated P-T Conditions, and Transect Measurements

Unit	Outcrop location	Peak T-P	Latitude	Longitude	Main foliation dip	Transect length (cm)	<i>n</i> veins	Vein%
LPU	1. Triplex	343°C ⁽¹⁾ – 1.5 GPa ⁽²⁾	44.998722	6.883972	N162 10°W	324.3	173	29.5
	2. Assietta	378°C ⁽¹⁾ – 1.8–1.9 GPa ^(2,3)	45.065819	6.953453	N130 60°E	334.3	95	22.0
	3. Château-Queyras	332°C ⁽⁴⁾ – 1.4 GPa ⁽²⁾	44.757933	6.793083	N145 33°W	355.8	65	32.4
	4. Malafosse	360°C ⁽²⁾ – 1.6 GPa ⁽²⁾	44.767472	6.831250	N170 25°W	185.7	41	13.3
	5. Gouret	366°C ⁽²⁾ – 1.7 GPa ⁽²⁾	44.787519	6.882408	N172 55°W	708.0	111	17.9
	6. Gouret	366°C ⁽²⁾ – 1.7 GPa ⁽²⁾	44.788583	6.887066	N164 45°W	897.9	149	20.6
LPM	7. Termignon	395°C ⁽⁵⁾ – 1.7 GPa ⁽²⁾	45.284556	6.834306	N038 40°N	151.7	37	12.1
	8. Lanslevillard	480°C ⁽⁶⁾ – 1.6–1.9 GPa ⁽⁶⁾	45.289833	6.906417	N096 37°N	264.3	61	10.3
	9. Mont-Cenis	435°C ⁽⁶⁾ – 1.6–1.9 GPa ⁽⁶⁾	45.259064	6.903197	N158 10°W	250.5	30	9.2
	10. Cerogne	387°C ⁽¹⁾ – 2 GPa ⁽²⁾	44.059042	6.984364	N169 15°W	254.0	51	22.6
	11. Balboutet	441°C ⁽¹⁾ – 2.2 GPa ⁽²⁾	44.062306	7.016667	N154 16°W	191.8	66	14.7
	12. Combe Morelle	388°C ⁽⁴⁾ – 2 GPa ⁽²⁾	44.764214	6.996486	N160 32°W	294.4	68	18.2

Note. P-T conditions were estimated from host-rocks in: ⁽¹⁾Beyssac et al. (2002), ⁽²⁾Herviou et al. (2022), ⁽³⁾Agard et al. (2001), ⁽⁴⁾Schwartz et al. (2013), ⁽⁵⁾Gabalda et al. (2009), and ⁽⁶⁾Plunder et al. (2012). Vein% correspond to the area of veins on each transect.

3d, 3e, and 3f; Caron, 1974; Herviou et al., 2021; Lefeuvre et al., 2020) and (b) Fe-Mg carpholite-bearing veins (Figure 3b; Agard et al., 2000, 2001; Goffé & Chopin, 1986; Raimbourg et al., 2018). Most of these veins relate to the D1 deformation stage (i.e., folded in a S1–S2 main foliation; Figures 3a–3h) and therefore record fluid circulation at prograde to peak burial of LPU and LPM units. These veins therefore allow studying fluid transfer at ~35–60 km depth in subduction zones (see Herviou et al., 2021).

4. Methodology

Twelve outcrops of blueschist-facies metasediments were selected from both the LPU and the LPM units (#1–6 and #7–12, respectively; Figures 2a and 3a–3h). These outcrops are located in Savoy, Cottian Alps and Queyras regions and contain rocks buried at P-T conditions fitting those of the deep SST environment (~330–380°C/1.4–1.9 GPa and ~390–480°C/1.6–2.2 GPa for the studied LPU and LPM outcrops, respectively; Figures 1a and 1b; Table 1). The location and peak P-T estimates for each outcrop are given in Table 1. The selected outcrops visually have slightly larger vein densities than the average Schistes Lustrés outcrop but are representative of the vein-rich outcrops encountered across the complex.

Vein distribution was quantified on 1D profiles for veins ≥1 mm-thick (Figures 3a–3h). For each outcrop, a representative linear transect, between ~150 and ~900 cm-long, was selected perpendicular to the main S1–S2 foliation (Figures 3a–3h, 2c, and 2d; Table 1), avoiding late D3-to-D5 veins. Vein spacings were measured from vein center to vein center. Measurement accuracy is approximately 1–2 mm and spatial resolution ~1 mm. Transects that were not strictly perpendicular to the main foliation were trigonometrically corrected for dip (outcrops #5, 6, 12). All measured veins are either occurring in folds marking an early S1 foliation or are located in the S1–S2 main foliation, consistent with their HP-LT origin (see below; Figures 3a–3h). Later folding of the D1 veins during D2 ± D3 deformation stages may however have affected their initial thicknesses and spacings (Figures 3b and 3c), as discussed below.

For all studied outcrops, vein distribution is shown by plotting each vein as a single line (Figure 4). Frequency-size plots are shown in Figures 8–10. Due to undersampling of the thinnest structures and the rare presence of large ones across short transects (André-Mayer & Sausse, 2007; Barton & Zoback, 1992; Gillespie et al., 1993; McCaffrey & Johnston, 1996; Monecke et al., 2001; Ortega et al., 2006; Pickering et al., 1995; Roberts et al., 1999; Sanderson et al., 1994, 2008), data sets tend to follow a characteristic concave-shape rather than a perfectly linear trend as expected for power-law distributions (e.g., Barton & Zoback, 1992; Blenkinsop, 1991; Braun & Kelemen, 2002; Gillespie et al., 1993; Ortega et al., 2006; Pickering et al., 1995). These truncation effects, commonly observed in vein and fracture data sets, tend to degrade the power law into negative exponential or log-normal distribution

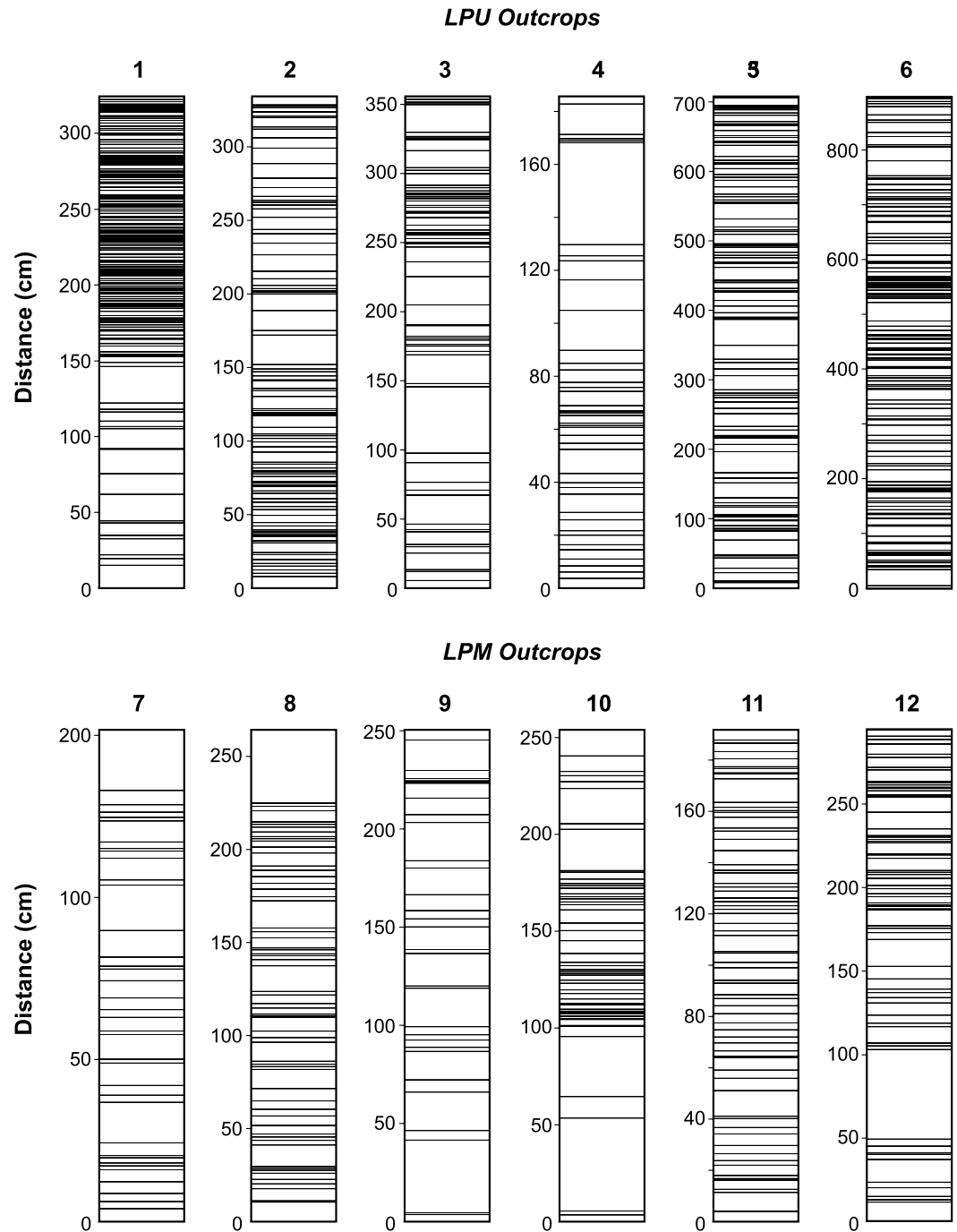


Figure 4. Vein distribution in the studied outcrops. Each line corresponds to a vein.

(e.g., Fagereng, 2011; Gillespie et al., 1993). The D dimension is then estimated along the central, linear segment of the curve (e.g., Braun & Kelemen, 2002). In our case it is also conspicuous that the successive stages of ductile deformation have affected the vein distribution across the studied outcrops (Figure 5), and significant deviations from power laws are expected.

Vein clustering, and its potential relationship with deformation features, was evaluated using the interval-counting technique of Manning (1994): each transect is divided into equal segments of length r , and the number of segments

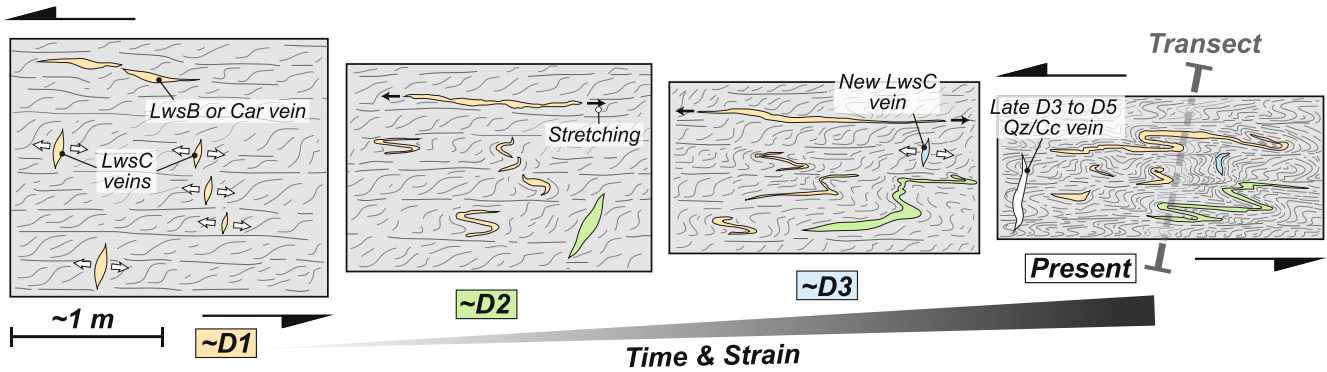


Figure 5. Simplified evolutionary sketch of the metamorphic veins deformation through time in the Schistes Lustrés outcrops from the D1 deformation stage at peak burial to the present setting. Measured transects are represented by a gray dashed line. Car: Fe-Mg carpholite; Cc: calcium carbonate; Lws: lawsonite; Qz: quartz.

$N(r)$ that contain at least one vein is recorded. After repetition for a range in r , the fractal dimension of clustering D_c correspond to: $D_c = (d(\log N(r)))/(d(\log 1/r))$. This method is equivalent to the box-counting technique used for 2D data sets (Barton, 1995; Barton & Larsen, 1985; Gillespie et al., 1993). Vein clustering was also quantified using the ratio of the standard deviation of spacings over the mean spacing (coefficient of variation Cv; e.g., Foxford et al., 2000; Gillespie et al., 1999).

Finally, the distribution of spacing between inclusion bands and trails in crack-seal veins (Ramsay, 1980) was measured, in order to quantify the displacement of each crack increment, and plotted in frequency-size graph to detect potential relationships with other statistical distributions. Previous works described exponential distributions (Fisher et al., 1995; Renard et al., 2005) and a characteristic length scale (Fagereng et al., 2011; Williams & Kirkpatrick, 2022) for the spacing between inclusion bands in crack-seal veins. In our crack-seal inclusions trails, spacing measurements were conducted from core to core of the solid inclusions. These measurements were realized by optical microscope observations and the use of an image processing software. Accuracy of measurement is around 0.5–1 μm . Abbreviations and symbols used in the following are given in Table 2.

5. Vein Patterns and Textures in the Schistes Lustrés

5.1. Field Observations

Metamorphic veins were tracked across the entire Schistes Lustrés complex (see Herviou et al., 2021). While blueschist-facies veins locally abound in both LPU and LPM units (Figures 3a–3h), larger amounts are observed in the LPU units than in the generally more carbonate-rich LPM metasediments. Across the 12 studied profiles, veins make up about 13%–32% of the LPU and 9%–23% of the LPM outcrops (Table 1). These calculations are consistent with estimations of Cartwright and Buick (2000) for the Schistes Lustrés of Alpine Corsica and those of Herviou et al. (2021) for the Schistes Lustrés of the Western Alps. In their study, Cartwright and Buick (2000) estimated that veins can make up to 30% of individual outcrops but that volumes of 5%–10% are most common. Herviou et al. (2021) estimated that high-pressure veins locally reach 20%–25% of individual outcrops. Several vein generations coexist in any of the Schistes Lustrés outcrop. While the exact chronological relationships might be obscured by later deformation, the presence of high-pressure minerals allows setting back veins within the D1/D2 deformation stages and in a simplified evolutionary sketch presented in Figure 5. Indeed, a significant proportion of the quartz veins measured in the field also contain minerals diagnostic of high-pressure conditions (i.e., lawsonite or Fe-Mg carpholite; Figures 6a–6f).

Lawsonite-bearing veins are by far the most abundant HP-LT veins in the Schistes Lustrés. Distinct types of lawsonite were described in the literature (Caron, 1974; Herviou et al., 2021; Lefeuvre et al., 2020) and the classification

Table 2
List of Symbols Used in This Study

Symbol	Meaning
t	Vein thickness
$N(t)$	Number of objects size t or greater
D_t	Fractal dimension of vein thickness
s	Vein spacing
$N(s)$	Number of objects size s or greater
D_s	Fractal dimension of vein spacing
D_c	Fractal dimension of vein clustering
Cv	Coefficient of variation
i	inclusion spacing
$N(i)$	Number of object size i or greater
D_i	Fractal dimension of inclusion spacing

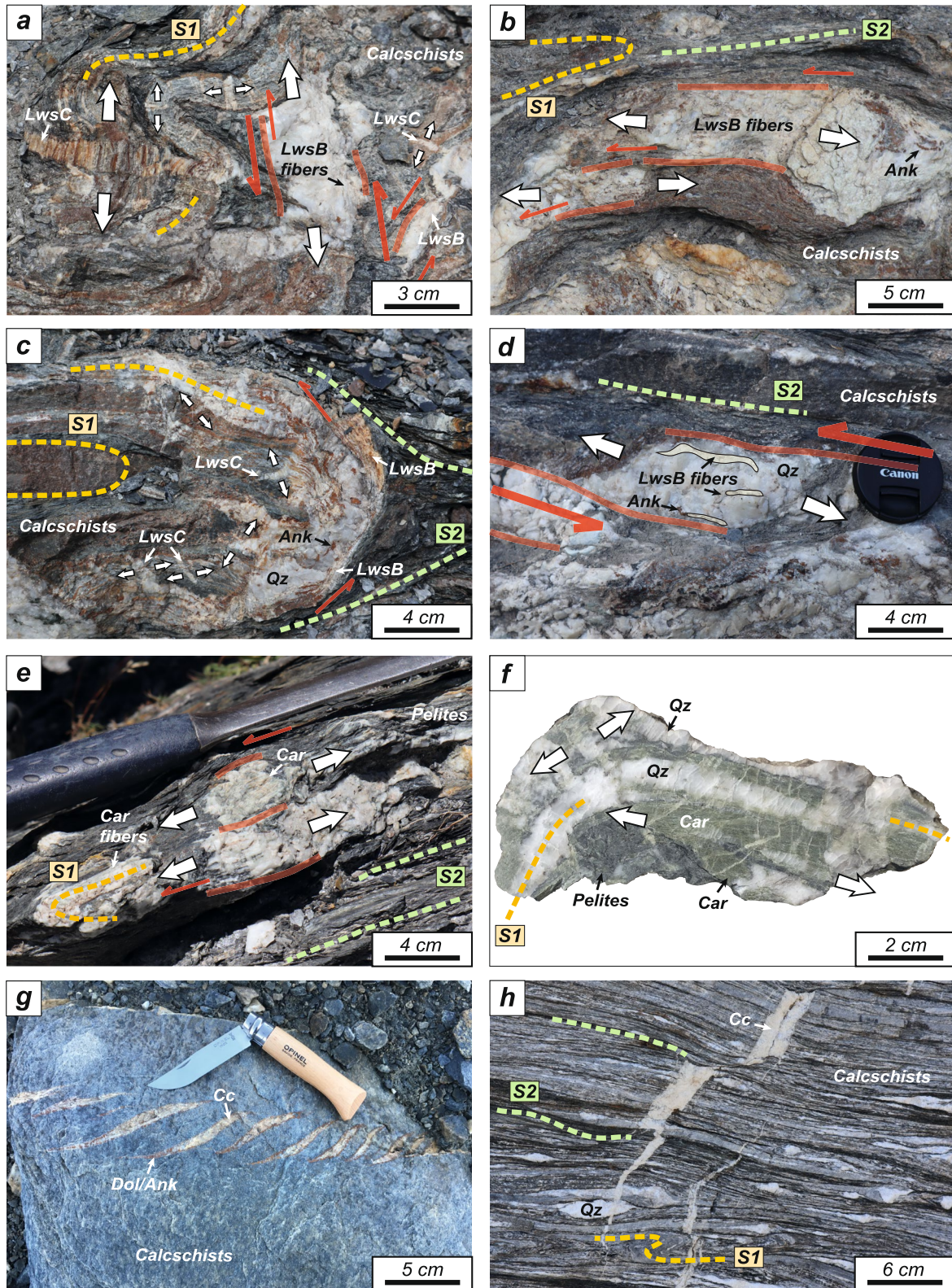


Figure 6. Metamorphic veins in the Schistes Lustrés with opening directions. (a–d) Syn-D1–D2 lawsonite B- and lawsonite C-bearing veins. (e and f) Syn-D1 Fe-Mg carpholite veins. (g and h) Syn D3-D4-D5 quartz- ± calcite, dolomite, albite and chlorite veins. Ank: ankerite; Car: Fe-Mg carpholite; Cc: calcium carbonate; Dol: dolomite; Lws: lawsonite; Qz: quartz.

of Lefeuvre et al. (2020) is used in the following. In contrast to the dark, organic matter-rich crystals of lawsonite in the schist (LwsA), two types of creamy-colored lawsonite-bearing quartz veins are observed: (a) pluri-cm- to m-long veins containing stretched crystals (in the sense of Bons et al. (2012)) of lawsonite oriented parallel to the vein walls (LwsB) and to quartz crystals (\pm minor ankerite; Figures 6a–6d); (b) mm- to cm-large tensional cracks containing lawsonite crystals, in textural equilibrium with ankerite and quartz, oriented perpendicular to the vein walls (LwsC; Figures 6a and 6c). LwsB veins outline D1 folds in places, advocating for early formation during prograde-to peak burial (Figures 3c–3e, 5, and 6a–6c), whereas LwsC cracks form during D1 and/or D2 (Figures 5, 6a, and 6c). In places where LwsB and LwsC veins coexist next to each other, LwsC veins are oriented at $\sim 80\text{--}90^\circ$ to LwsB veins but LwsB and LwsC crystals are oriented in the same direction (Figures 6a and 6c).

Though more sensitive to retrogression than lawsonite and therefore scarcer at present, Fe-Mg carpholite-bearing veins are also observed in the Schistes Lustrés metasediments, with similar features to LwsB veins for most of them (Figures 3b, 6e, and 6f). As for lawsonite-bearing veins, they markedly differ from the late-stage greenschist-facies D3/D4/D5 veins filled with quartz \pm calcite, dolomite, albite and chlorite, that crosscut the main S1–S2 foliation (Figures 5, 6g, and 6h).

5.2. Observations at the Microscopic Scale

At the microscopic-scale too, LwsB, LwsC and Fe-Mg carpholite-bearing veins contain stretched crystals of lawsonite or Fe-Mg carpholite in textural equilibrium with quartz \pm ankerite crystals (Figures 7a–7h; see Herviou et al., 2021; Lefeuvre et al., 2020 for more pictures on their textural relationships).

In LwsB and LwsC veins, quartz crystals preserved from dynamic recrystallization host successive trails of regularly spaced (micrometric) idiomorphic lawsonite crystals, with a similar aspect ratio along each trail (Figures 7a–7d). These solid inclusion trails, oriented parallel to the stretched lawsonite crystals, are characteristic of vein opening by a crack-seal mechanism through repeated fracturing and sealing events under high fluid pressure (Cox, 1987; Ramsay, 1980). Each crystal is considered to correspond to one increment of tensional opening and the thickness of quartz between successive lawsonite crystals is interpreted as the amount of opening for one crack increment.

In crack-seal veins, “inclusion bands” are planes of solid and/or fluid inclusions located perpendicular to the opening direction and interpreted as sealed microcracks (Fagereng et al., 2011; Fisher & Brantley, 1992, 2014; Fisher et al., 1995; Ramsay, 1980; Renard et al., 2005; Ujiie et al., 2018). Such bands were not observed in quartz crystals associated with LwsB and LwsC veins, probably due to removal during quartz recrystallization. Yet, lawsonite crystals which are better preserved from dynamic recrystallization than quartz contain successive trails of aqueous two-phase (liquid + vapor) fluid inclusions (Figures 7e and 7f). Since they are oriented perpendicular to the stretched crystals and show a micrometer-sized spacing matching that of the lawsonite inclusion trails in quartz crystals (Figures 7a–7f), they are interpreted as crack-seal inclusion bands.

In Fe-Mg carpholite-bearing veins, successive inclusion bands, similar to those of LwsB and LwsC veins were observed in Fe-Mg carpholite (Figure 7g) and in quartz crystals (Figure 7h). These bands mostly contain aqueous two-phase (liquid + vapor) fluid inclusions and are oriented perpendicular to stretched fibers and therefore to the opening direction.

6. Results

6.1. Vein Thickness Distribution

In the studied transects, measured vein thicknesses vary between 0.1 and 24 cm. The mean and median vein thickness ranges are 0.4–1.2 cm and 0.2–0.5 cm, respectively (Table 3) highlighting the presence of many thin veins <1 cm. The mean/median thickness of veins from all outcrops, all LPU outcrops and all LPM outcrops are respectively 0.9/0.3 cm, 1/0.3 cm, and 0.7/0.2 cm.

The statistical distribution of veins for a given outcrop, as well as for all outcrops, is not linear (Figures 8a and 8b; Figure S1 in Supporting Information S1; for symbol descriptions see Table 2). Frequency-size plots in log-linear scale are characterized by a non-linear trend showing that vein thickness distributions are not well described by log-normal or exponential laws (Figure S1 in Supporting Information S1). Finally, most of the

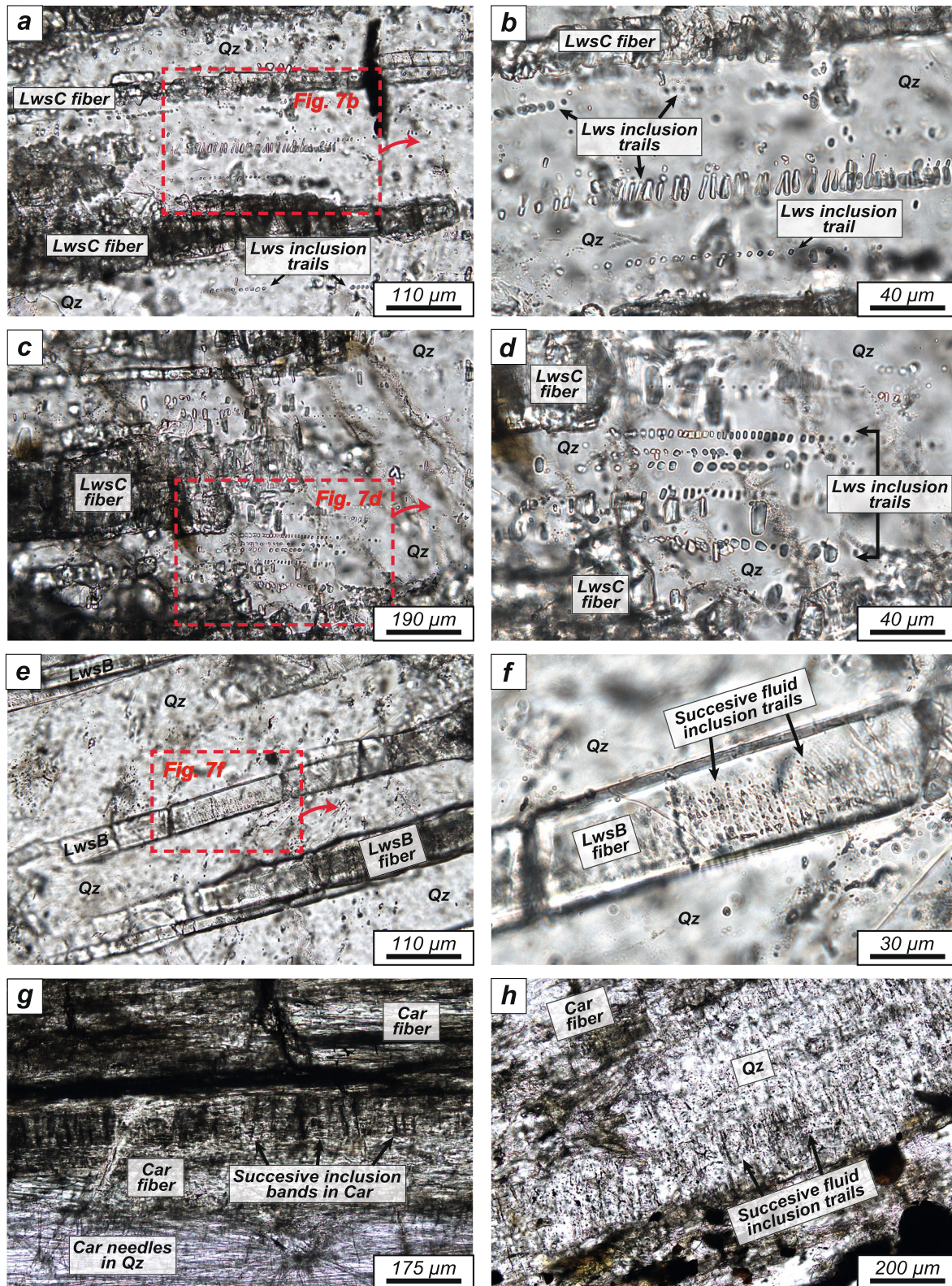


Figure 7. Crack-seal textures in lawsonite- and Fe-Mg carpholite-bearing veins. (a–d) Successive lawsonite inclusion trails in quartz in textural equilibrium with Lawsonite C stretched crystals. (e and f) Successive trails of fluid inclusions in a lawsonite B fiber. These trails are considered as equivalents to Ramsay (1980) crack-seal bands. (g) Crack-seal bands made of fluid and solid inclusions in a Fe-Mg carpholite crystal. (h) Successive fluid inclusions trails in quartz in textural equilibrium with Fe-Mg carpholite crystals. Car: Fe-Mg carpholite; Lws: lawsonite; Qz: quartz.

Table 3
Statistical Data on Vein Distribution (Vein Thickness, Vein Spacing, and Vein Clustering)

Outcrop	Mean thick. (cm)	Med. thick. (cm)	Sd thick. (cm)	Mean spac. (cm)	Med. spac. (cm)	Sd spac. (cm)	D_t	R^2	D_s	R^2	Cv spac.	D_c	R^2
All outcrops	0.9	0.3	1.8	4.4	2.4	5.8	1.24–1.32	0.935–0.987	1.31	0.979	1.31	/	/
All LPU outcrops	1.0	0.3	2.1	4.4	2.3	5.6	1.15–0.97	0.934–0.975	1.58	0.992	1.27	/	/
All LPM outcrops	0.7	0.2	1.2	4.5	2.7	6.2	1.20–0.93	0.935–0.984	1.33	0.992	1.38	/	/
1	0.6	0.2	1.7	1.9	1.1	3.1	1.05	0.968	1.72	0.984	1.68	0.79	0.996
2	0.8	0.2	1.5	3.5	2.6	3.3	0.96	0.954	1.17	0.962	0.94	0.60	0.984
3	1.8	0.5	3.8	5.5	2.5	7.6	0.78	0.965	0.72	0.994	1.38	0.60	0.976
4	0.6	0.2	0.9	4.5	2.8	6.3	0.96	0.944	1.21	0.988	1.39	0.78	0.984
5	1.1	0.5	1.6	6.4	4.2	6.4	1.01–0.99	0.912–0.981	1.71	0.991	1.00	0.66	0.976
6	1.2	0.4	2.2	6.0	4.1	6.1	0.92–0.74	0.903–0.987	1.72	0.984	1.02	0.65	0.984
7	0.5	0.2	0.9	4.1	2.8	3.9	0.94	0.972	1.26	0.977	0.96	0.56	0.931
8	0.4	0.2	0.6	3.7	2.5	3.2	1.21	0.910	1.28	0.980	0.87	0.86	0.978
9	0.8	0.2	1.3	8.2	4.15	8.2	0.79	0.957	0.79	0.958	1.00	0.46	0.928
10	1.1	0.4	1.9	5.0	2.3	8.4	0.78–0.58	0.906–0.984	0.92	0.989	1.68	0.63	0.979
11	0.4	0.2	0.7	2.8	2.7	1.9	1.08	0.992	2.48	0.981	0.67	0.61	0.967
12	0.8	0.4	1.3	4.3	2.25	6.9	0.99	0.937	0.89	0.985	1.60	0.81	0.986

Note. In some outcrops, vein thicknesses are affected by truncation artifacts (All outcrops, all LPU, all LPM, outcrops #5, 6, 10). For these outcrops D_t and R^2 value are presented for all the data set (left of the hyphen) and for the central linear section of the data set (right of the hyphen).

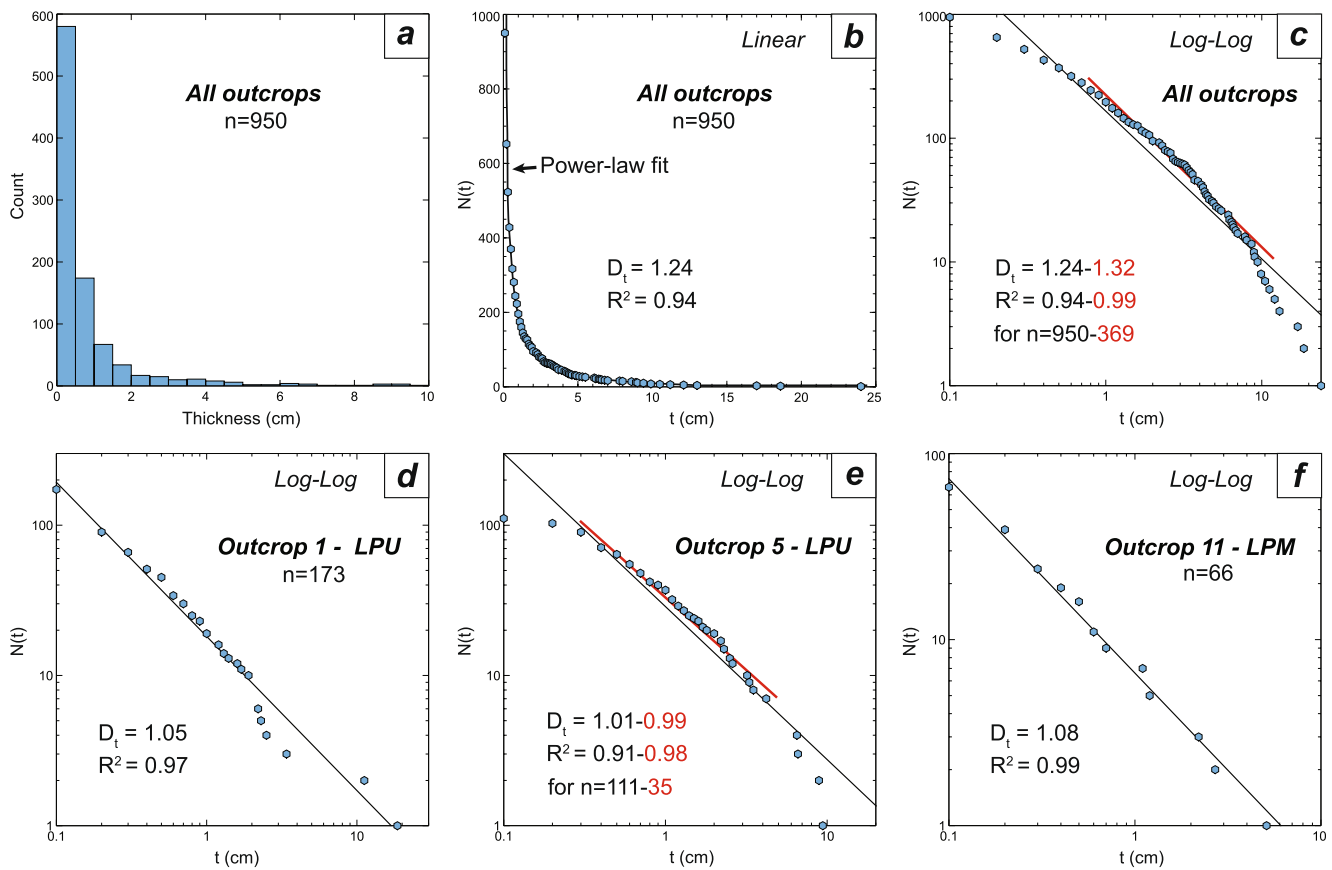


Figure 8. Vein thickness distribution. (a) Histogram of all measured vein thicknesses. (b) Frequency-size plot in linear scale of all measured vein thicknesses and fit with a power law (black curve). (c–f) Frequency-size plots in log-log scale of thicknesses of all outcrops (c), and of representative outcrops (d–). Lines correspond to linear regressions in log-log scale and therefore fits with power laws. Black lines correspond to power law fits for all measures while red lines correspond to power law fits for a range of values in truncated data sets.

frequency-size plots in log-log scale exhibit linear trends with coefficients of determination greater than 0.91 (R^2 ; Figures 8c–8f; Figure S1 in Supporting Information S1), suggesting that vein thicknesses are well described by a power-law distribution. For some outcrops as for compiled data sets (all outcrops, all LPU outcrops and all LPM outcrops), the frequency-size plots in log-log scale show a relatively concave shape characteristic of truncated power-law distributions (Figures 8c and 8e; e.g., Gillespie et al., 1993; see Section 4), reflecting the fact that very thin veins could not be measured and large ones may have been missed. The initial power law distribution achieved during vein formation might also have been affected by the successive stages of ductile deformation (Figure 5).

The range of fractal dimension for vein thicknesses D_t is 0.74–1.05 in LPU outcrops and 0.58–1.21 in LPM outcrops (Table 3). Values of D_t are 1.32, 0.97, and 0.93, when considering all outcrops, all LPU outcrops and all LPM outcrops, respectively (Table 3). Nearly all transects have very close D_t values (around 1), suggesting comparable proportions of thick and thin veins among the different outcrops (Table 3). Outcrop 10 has a D_t value of 0.58 showing the greatest proportion of thick veins in this outcrop, whereas outcrop 8 with a D_t of 1.21 has the greatest proportion of thin veins (Table 3).

6.2. Vein Spacing Distribution

As with thicknesses, vein spacings vary largely, between 0.1 cm (resolution of the method, see Section 4) and 53.6 cm. The mean and median spacing ranges for outcrops are respectively 1.9–8.2 cm and 1.1–4.2 cm (Table 1). The mean/median space between veins from all outcrops, all LPU outcrops and all LPM outcrops are quite similar (4.4/2.4 cm, 4.4/2.3 cm, and 4.5/2.7 cm, respectively).

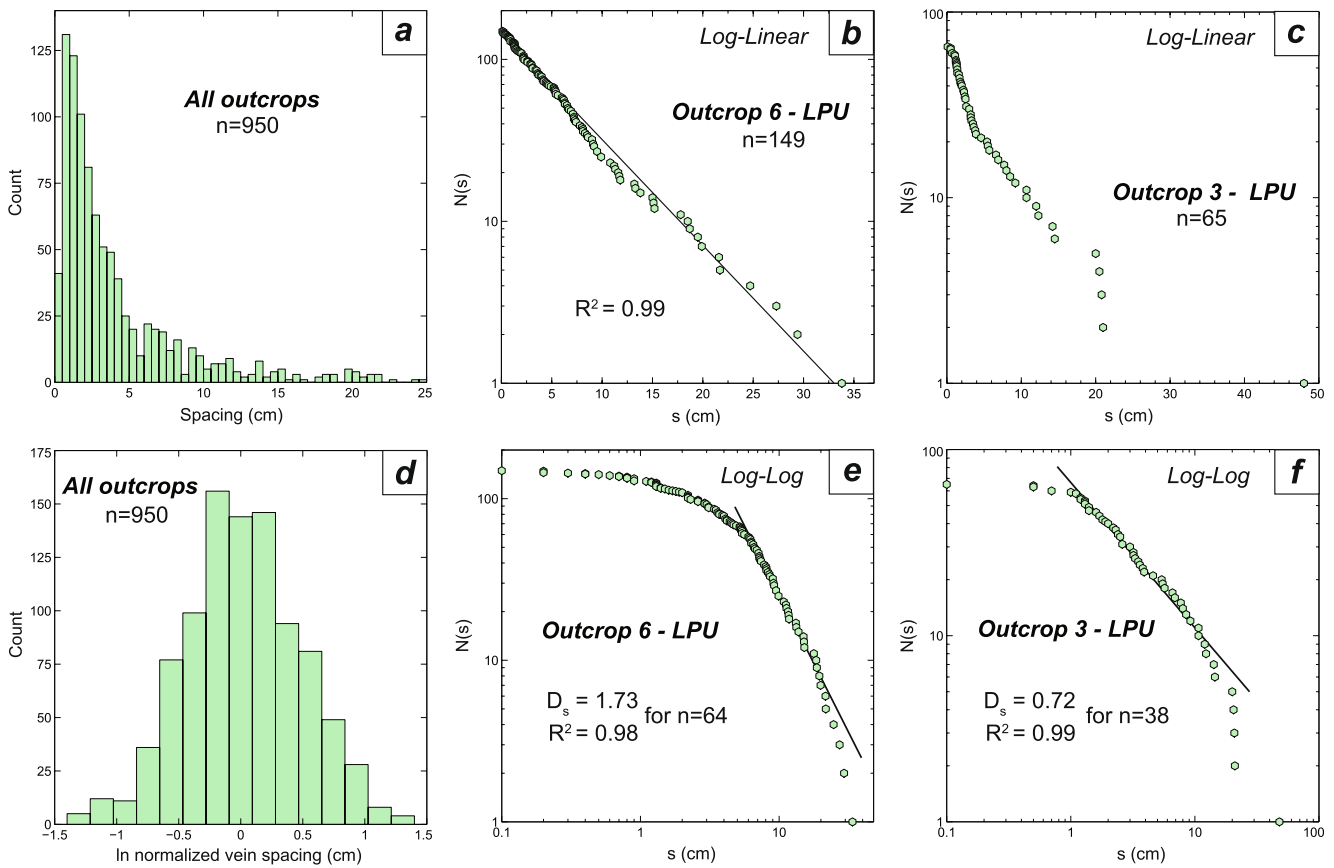


Figure 9. Vein spacing distribution. (a) Histogram of all measured vein spacings. (b and c) Frequency-size plots of vein spacings in log-linear scale for two outcrops. The black line in (b) correspond to a linear regression in log-linear scale and therefore to a fit with a log-normal or exponential law. (d) Histogram of the natural logarithm of normalized vein spacing (each spacing divided by median spacing). (e and f) Frequency-size plots of vein spacings in log-log scale for two outcrops. Linear regressions correspond to fit with power laws for the central linear part of these truncated data sets.

The statistical distribution of spacing is not linear, as shown by cumulative histograms and frequency-size plot (Figure 9a; Figure S2 in Supporting Information S1). These plots highlight the dominance of small spacings, yet with a lesser amount of spacings <0.5 cm (Figure 9a), suggesting a poor fit with power laws. In log-linear scale, some frequency-size plots show a nice linear trend suggesting that vein spacings have a good fit with log-linear or exponential distributions (Figure 9b). Conversely, some outcrop frequency-size plots rather have a concave-shape (Figure 9c), demonstrating that the distribution of vein spacing does not correspond to log-linear or negative

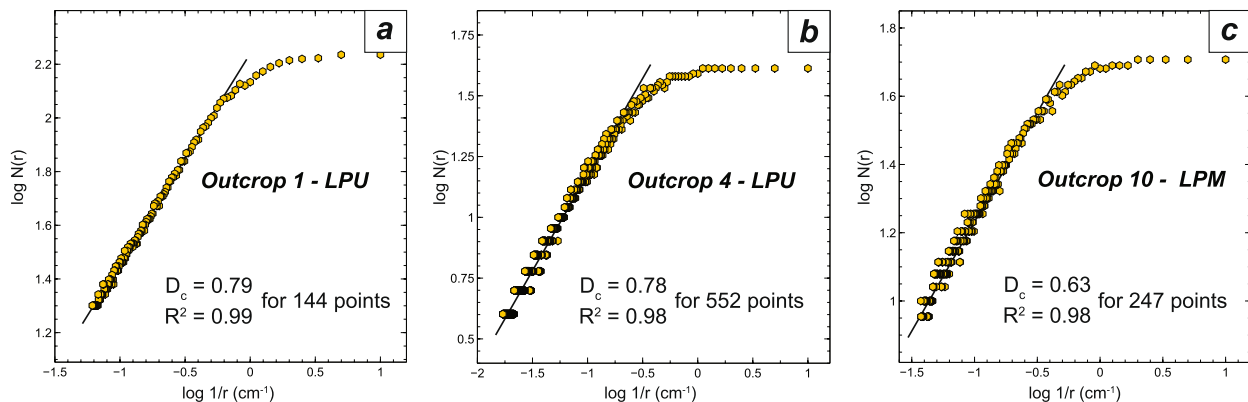


Figure 10. (a–c) Vein clustering for three representative outcrops, following the methodology of Manning (1994). Black lines correspond to fits with power laws for the linear part of these truncated data sets.

exponential distributions. The cumulative histogram of the natural logarithm of normalized vein spacing (each spacing divided by median spacing) for all outcrops has an almost symmetric shape, suggesting that spacings follow a log-normal distribution (Figure 9d; Narr & Suppe, 1991)—contrary to single outcrops (Figure S2 in Supporting Information S1). Frequency-size plots of spacings in log-log scale have a concave shape with a central linear part (Figures 9e and 9f) suggesting that, as for vein thicknesses, spacings potentially had an initial power law distribution affected by truncation of both small and large spacings (Barton & Zoback, 1992; Fagereng, 2011; Gillespie et al., 1993; Pickering et al., 1995) and by the successive stages of ductile deformation.

The fractal dimension of vein spacings D_s is thus calculated by linear regression on the central linear part of the curves (Figures 9e and 9f). All coefficients of determination are greater than 0.96 (Table 3), and nearly always greater than those calculated in log-linear scale (Figure S2 in Supporting Information S1). The range of D_s is 0.72–1.72 in LPU units and 0.79–2.48 in LPM units (Table 3), and 1.31, 1.58, and 1.33 for all, all LPU, and all LPM outcrops data sets, respectively (Table 3). Changes in D_s values reflect differences in the proportions of thin and thick spacings, and greater D_s value correspond to a greater proportion of small spacings. The variation of these fractal dimensions (0.72–2.48; Table 3) points to significant differences in vein spacings among outcrops. With D_s values lower than 1, outcrops #3, 9, 10, and 12 have a much greater proportion of large spacings than the others where D_s are greater than 1 (Table 3). Outcrops #2, 4, 7, and 8 showing D_s around 1.2–1.3 have comparable proportion of small and large spacings (Table 3). With D_s values around 1.7, outcrops #1, 5, 6 also have a comparable number of large and small spacings, yet with a greater proportion of thin spacings than outcrops #2, 4, 7, and 8. Finally outcrop #11, with a D_s value of 2.48, has the greatest proportion of small spacings amongst all studied outcrops.

6.3. Vein Clustering

Using the method of Manning (1994; see Section 4), frequency size plots of $\log N(r)$ versus $\log (1/r)$ show curved tendencies (Figures 10a–10c; Figure S3 in Supporting Information S1) as for vein spacing distributions and some vein thickness distributions (Figures 8c, 8e, 9e, and 9f). Most of the points of these plots show a linear trend up to a high $\log N(r)$ and high $\log (1/r)$ value where the slope changes to a concave shape (Figures 10a–10c). High $\log (1/r)$ values correspond to segments of small length r , the break in slope then occurs for a high number (high $N(r)$) of small divisions of the transects. This suggest that as the size of segments gets closer to the minimum vein spacing and thickness, the number of boxes containing at least one vein stops increasing because of truncation of small veins and small spacings (Stowell et al., 1999). The fractal dimension of clustering D_c can be calculated for the linear sections of the trends, for which coefficients of determination are greater than 0.93 (Table 3).

D_c values provide a direct information on how veins cluster in outcrops, with an increase of D_c reflecting an increasing filling of space by veins and a decreasing clustering (Barton, 1995; Fagereng, 2011; Magde et al., 1995; Manning, 1994). For intersection of veins with a transect, the distribution is fractal if $0 < D_c < 1$ (Manning, 1994). If D_c is equal to 0.5, the spacing of veins is uncorrelated; from 0.5 to 0 the veins are increasingly clustered (Barton, 1995), whereas from 0.5 to 1 veins are less clustered and more evenly spaced (Barton, 1995). The mean D_c for the LPU and LPM outcrops are 0.68 and 0.65 respectively, suggesting only low clustering and a relatively uniform spacing of veins. For single outcrops, D_c values are in the range of 0.60–0.79 and 0.46–0.86 for LPU and LPM, respectively (Table 3), showing subtle variations of clustering. With a D_c of 0.46, outcrop #9 shows a modest yet the greatest clustering of all transects, whereas outcrops #1, 4, 8, and 12 are the least clustered (0.78–0.86; Table 3).

The coefficient of variation (ratio of standard deviation to the mean) of vein spacings C_v (see Table 2) provides an additional evaluation of clustering (Cox & Lewis, 1966; Fagereng, 2011; Foxford et al., 2000; Gillespie et al., 1999; Lahiri et al., 2020; McCaffrey & Johnston, 1996): $C_v = 0$ if veins are equally spaced; $C_v = 1$ for a random/independent distribution; $C_v > 1$ if veins are clustered; $C_v < 1$ if they are unclustered. Combined data sets yield 1.31, 1.27, and 1.38 for all, all LPU and all LPM outcrops, respectively. Five over twelve transects (outcrops #1, 3, 4, 10, 11; Table 3) have $C_v > 1$, indicating that veins are somewhat clustered. Three outcrops (#5, 6, and 9; Table 3) have C_v spacings close to 1, indicating random distributions, and the four remaining ones (#2, 7, 8, 11; Table 3) have $C_v < 1$, indicating anticlustered and regularly spaced veins.

Yet the evaluation of clustering obtained via D_c and C_v only weakly correlates in the different outcrops (Table 3). This misfit was already observed (Fagereng, 2011) and is likely an artifact of the two different data sets considered

Table 4
Statistical Data on Crack-Seal Inclusion Bands and Trails in Lawsonite-Bearing Veins

Vein type	Inclusion type	<i>n</i> measurements	Mean spac. (μm)	Med. spac. (μm)	Sd spac. (μm)	<i>D_i</i>	<i>R</i> ²
LwsC	Lws inclusion trails	432	6.3	5.5	3.9	2.72	0.989
LwsB	Lws inclusion trails	139	5.4	5.3	2.7	2.33	0.992
	Fluid inclusions trails	100	5.3	4.9	2.5	2.31	0.987
	Lws + fluid inclusions trails	239	5.4	5.0	2.6	2.67	0.993
LwsC + LwsB	Lws + fluid inclusions trails	671	6.0	5.3	3.5	2.82	0.993

Note. Lws: lawsonite.

for these calculations. Because of truncation artifacts, only a range of *r* was considered to obtain *D_c*, whereas *C_v* was obtained from the entire data set, despite the fact that spacing distributions are also affected by truncation (see Section 4). We therefore consider that *D_c* provides a better measure of clustering for our data sets.

6.4. Crack-Seal Inclusion Spacing Distribution

The spacings between lawsonite inclusion trails were measured in one sample of LwsC vein and one sample of LwsB vein where crack-seal textures were particularly well preserved (Figures 7a–7d; Section 5.2). The spacings between fluid inclusions trails, interpreted as inclusions bands, were measured in lawsonite crystals of the same LwsB vein (Figures 7e and 7f; Section 5.2). In these different trails and bands, the mean/median spacings are 6.3/5.5 μm, 5.4/5.3 μm, and 5.3/4.9 μm in lawsonite inclusion trails of the LwsC vein (*n* = 432), lawsonite inclusion trails of the LwsB vein (*n* = 139) and fluid inclusion bands of the same LwsB vein (*n* = 100; Table 4), respectively. These very similar results for the three microstructures suggest that they may have formed through the same process.

All frequency-size plots and cumulative histograms are shown in Figure S4 of the Supporting Information S1. The distribution of inclusion spacing is not linear (Figures 11a and 11b), and some plots show fairly linear trends in log-linear scale, suggesting a possible good fit with log-normal or exponential laws, as already shown in inclusion bands from crack-seal veins (Fisher et al., 1995; Renard et al., 2005). With standard deviation representing a relatively close range of the mean (~46–62% of the mean for the three studied microstructures; Table 4), the presence of a characteristic length scale for inclusion band/trail spacings seems possible (Fagereng et al., 2011; Williams & Kirkpatrick, 2022). Some of the log-linear frequency-size plots are however going against log-normal/exponential distributions with their non-linear trends (Figure 11c). In log-log scale, frequency-size plots show concave trends, again with a fairly linear central section, and with a significant change in slope for small spacings (Figures 11d–11f). The smallest spacings were challenging to measure because some lawsonite inclusions have grown enough to fill the quartz gap between each other, making it difficult to assert if inclusions are made of one of two crystals (Figures 11a–11d). Given that small inclusion spacings have likely been missed due to measurement limitations, the spacings might follow a somewhat truncated power-law distribution. Therefore, the central linear section of the log-log frequency-size plots was used to estimate the fractal distribution of inclusion spacings *D_i* (see Table 2). Coefficients of determination are 0.99 for a significant part of the inclusion spacings (Figures 11d–11f). The *D_i* value corresponds to the proportion of large versus small increments of displacement. *D_i* values are 2.72, 2.33, and 2.31 for lawsonite inclusion trails of the LwsC vein, lawsonite inclusion trails in the LwsB vein and fluid inclusion bands in the same LwsB vein, respectively (Table 3).

7. Discussion

7.1. Mechanisms of Vein Formation in the Schistes Lustrés

The blueschist-facies Schistes Lustrés metasediments contain high-pressure veins, either millimeter- to centimeter-long with mineral fibers perpendicular to the vein walls (LwsC veins), or decameter- to meter-long with mineral fibers parallel to the vein length (LwsB veins; part of the Fe-Mg carpholite-bearing veins; Section 5.1). While LwsC veins are readily interpreted as tension gashes formed by local extension through mode I fracturing, the formation of LwsB veins with lawsonite crystals parallel to the vein length is more enigmatic.

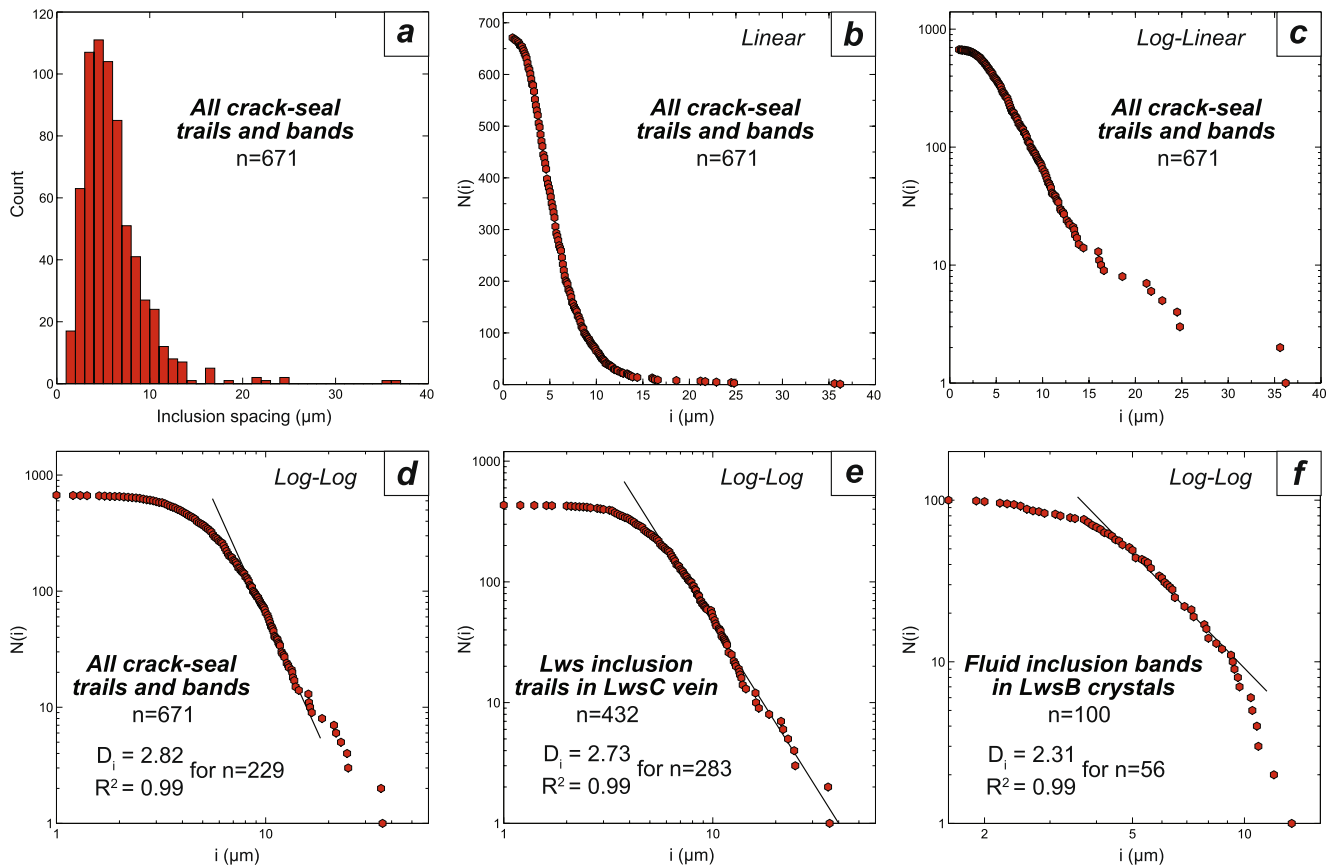


Figure 11. Spacings between crack-seal inclusion trails and bands. (a) Histogram of all measured spacings between crack-seal bands and trails in lawsonite-bearing veins. (b and c) Frequency-size plots of spacings between crack-seal bands and trails in lawsonite-bearing veins in linear and log-linear scales. (d–f) Frequency-size plots of spacings between crack-seal bands and trails in lawsonite-bearing veins in log-log scale. Black lines correspond to fits with power laws on the linear part of these truncated data sets. Lws: lawsonite.

Yet, in places where LwsB and LwsC veins coexist next to each other, LwsC veins are oriented at $\sim 80\text{--}90^\circ$ to LwsB veins, that is, crystals are oriented in the same direction, suggesting that these two types of veins may have formed under the same stress regime and possibly coevally (Figures 6a–6d). LwsB veins would thus form through incremental stretching and fiber growth during ductile deformation, in pressure shadows of rigid objects or by progressive opening under brittle failure.

This conclusion is strengthened by the existence of successive trails of lawsonite crystals parallel to the fibers in LwsB and LwsC veins, and by fluid inclusion bands perpendicular to crystal fibers in both lawsonite- and Fe-Mg carpholite-bearing veins (Section 5.2; Figures 7a–7f). Collectively, these observations show that LwsB-, LwsC- and Fe-Mg carpholite-bearing veins formed as crack-seal veins (Cox, 1987; Ramsay, 1980) through repeated cycles of fracturing and mineral growth under high fluid pressure, with an opening direction parallel to the macroscopic fibers of lawsonite and Fe-Mg carpholite (Figure 12).

In the LwsB and elongate Fe-Mg carpholite-bearing veins best preserved from later folding of the S1 foliation, the roof and ground walls are sharp (Figures 6a, 6b, and 6d) and shear senses can be observed at the contacts between the veins and the wall-rock. This suggests that fractures opened under mode II shear failure (Figure 6d), and that these veins formed by local extension between faults or shear planes in cm-scale pull-aparts (Figure 12), as suggested by Fagereng et al. (2010, 2011; see also Bons et al., 2012; Lemonnier et al., 2020).

The elongate high-pressure mineral-bearing veins studied here thus likely formed along weak cleavage/foliation planes (similar to Fagereng et al., 2010; Figure 12), during prograde to peak burial under the dominant subduction zone shear regime (Figures 13a and 13b). Incremental crystal growth along the long axis of the vein reflects the strength ratio contrast between the matrix and the growing vein (e.g., LwsB vein), deformation being partitioned

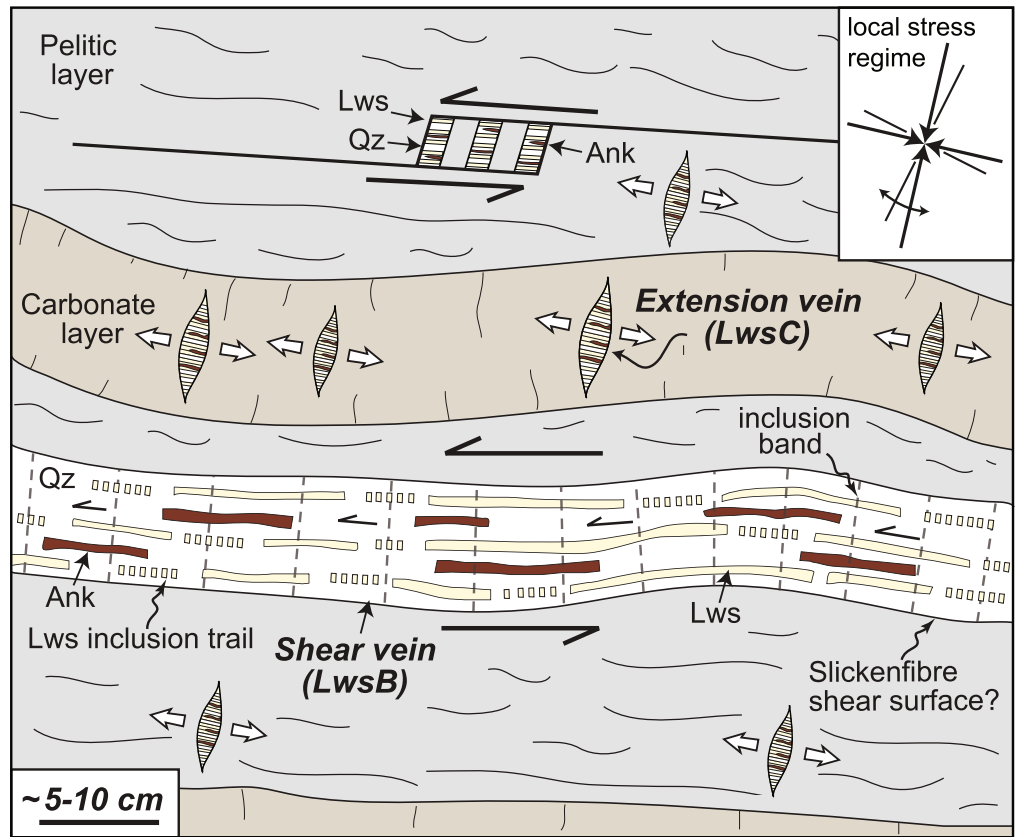


Figure 12. Schematic drawing of the geometrical relationship between shear and extension veins, and the inferred mechanisms for vein formation. Inferred instantaneous local stress regime is in the top right. Modified after Fagereng et al. (2010).

between distributed dissolution-precipitation creep in the matrix and brittle opening along the relatively stronger growing vein.

The similar spacings and D_i values between the crack-seal textures (trails and bands) of LwsB and LwsC veins (Table 4; Section 6.4) suggest that at least some of the small veins classified as LwsC also formed incrementally along small pull-apart jogs, rather than as tension gashes (Figure 12). They may correspond to small abandoned shear increments while LwsB pull-apart veins would therefore correspond to long-lived structures built through successive shearing events along or close to the subduction interface, downdip of the seismogenic zone (Figures 12 and 13b).

7.2. Vein Distribution in the Schistes Lustrés and Implications for Fluid Flow

Vein thicknesses follow relatively well-defined power-law distributions, despite minor deviations in some outcrops (Figures 8a–8f; Section 6.1). Vein spacings, vein clustering and inclusion spacings show instead significant deviations from power-law distributions, as previously reported and commonly interpreted as the result of truncation artifacts (e.g., Gillespie et al., 1999; Figures 9a–9h, 10a–10h, 13b, and 13c; Sections 6.2–6.4). However, in contrast to almost all previous studies of vein distribution (e.g., Clark et al., 1995; Fisher et al., 1995; Sanderson et al., 1994; see Section 2), our veins did not form by extension along the measured transects, but through foliation-parallel incremental growth (i.e., perpendicular to the transects; Section 7.1). Therefore, the power-law distribution of vein thicknesses and spacings cannot be ascribed to the accommodation of general extension by nucleation and growth of veins (unlike Clark et al., 1995). A second consequence is that the extent to which the polyphase deformation of the Schistes Lustrés metasediments may have modified vein thicknesses/spacings (Figures 5 and 13c) and fractal dimensions must be assessed. The distribution of vein thickness (green arrows in Figures 13b and 13c) and spacing/clustering (black arrows in Figures 13b and 13c) were likely fractal and potentially inherited from a fractal distribution of preexisting weak planes where deformation localized

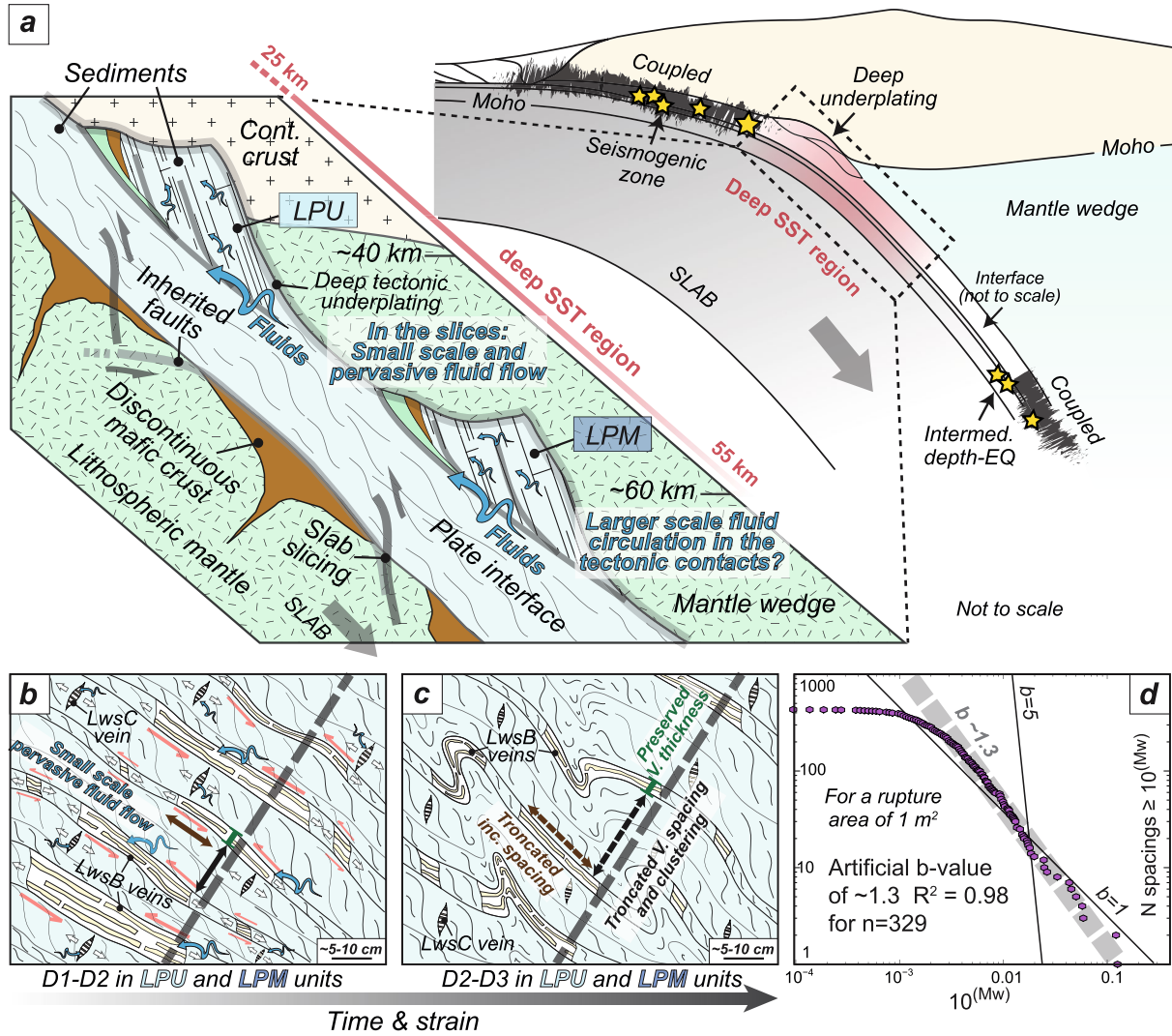


Figure 13. Fluid flow and deformation processes at the downdip end of the seismogenic zone. (a) Schematic drawing of a subduction zone with focus on the subduction interface at the depth of deep SST nucleation and LPU-LPM units peak burial (~25–55 km depth). A pervasive circulation of fluids at the peak burial of the tectonic slices is suggested by vein distribution and geochemical studies. A much larger scale and more channelized fluid flow is expected along the tectonic contacts. (b) Formation of high-pressure crack-seal veins during D1–D2 deformation stages at conditions close to peak burial. Lawsonite B-bearing veins such as most of the Fe-Mg carpholite veins formed by dilational shearing between weak planes while lawsonite C-bearing veins either formed by mode I extensional fracturing or correspond to small abandoned shear increments comparable to lawsonite B-bearing veins. During these deformation stages, the fluid flow responsible for vein formation was pervasive and limited in scale (m-hm scale at most). The distributions of vein thickness (green arrow) and spacing/clustering (black arrow) were fractal and potentially inherited from fractal distributions of preexisting weak planes (joint/fracture/stylolitic planes) where strain localized to form veins. The spacings of crack-seal inclusions (brown arrow) were also fractal, reflecting fractal slip increments potentially related to slow slip and tremor events. (c) Folding of the high-pressure veins during D2–D3 deformation stages. The lawsonite- and Fe-Mg carpholite-bearing veins were intensively deformed during exhumation, which may have affected the distribution of vein spacings (black dotted arrow) and inclusion spacings (brown dotted arrow) while the fractal distribution of vein thicknesses was preserved (green arrow). Truncation artifacts affected the original fractal distribution of vein and inclusion spacings. Gray dashed lines on (b) and (c) correspond to the measured transects. (d) Frequency-magnitude relationship estimated for inclusion trail spacings in lawsonite-bearing crack-seal veins considering a rupture of 1 m². The obtained fractal dimension of 1.3 is similar to the *b*-value of some slow slip events, to ordinary subduction earthquakes (both often having *b*-value around 1). This value is lower than the *b*-value obtained for low-frequency earthquakes when a power law distribution is favored (*b*-value ≥ 5, at least for the large ones) but may be compatible with small low-frequency earthquakes suggesting that the studied veins may correspond to the record of successive small low-frequency earthquakes in subduction. EQ: earthquakes; LPU: Liguro-Piemont Upper units; LPM: Liguro-Piemont Middle units; LPL: Liguro-Piemont Lower units; SST: slow slips and tremors; V.: vein.

to form veins (Figure 13b). Stylolitic cleavage planes or joint/fracture planes indeed tend to follow power-law distributions too (Barton & Zoback, 1992; Hooker et al., 2013; La Pointe, 1988; Ledésert et al., 1993; Velde et al., 1990, 1991; Figure 13b).

Folding and cumulative deformation may have “multiplied” the number of veins along the measured transects, thereby affecting vein density and vein spacings (Figure 5). Thicknesses may also have been modified through folding, stretching (boudinage) and/or distributed pressure-solution processes (Gratier et al., 2013). Whether pressure-solution was distributed homogeneously or not, either across the outcrop, or between the veins and host rocks is unknown. No contrast in the amount of dissolution can be observed between the thin and thick veins along the vein walls, such that the distribution of vein thickness was either not modified too significantly or shifted homogeneously (Figures 5 and 13c). This conclusion is even more valid for clustering. In contrast, the distribution of vein spacing is more uncertain, since it depends on the strain localization history. Despite these caveats, it is unlikely that later deformation generated the power-law distributions retrieved in our data sets. Furthermore, since all the studied transects were affected by the same deformation events, it is possible to compare the statistical distributions of similar veins lying along the composite S1–S2 foliation (Section 4; Figures 5, 13b, and 13c).

Calculated distributions for combined data sets show that the studied outcrops have a great proportion of thin veins (power-law distributions with D_t greater or close to 1 and mean thickness around 1 cm; Table 3) and thin spacings (power-law distributions with D_s greater than 1; mean spacing around 4.5 cm; Table 3). This suggests that fluids mostly circulated pervasively through the rock rather than along major localized conduits (Figures 13a and 13b). Moreover, the mean D_c of 0.67 for all studied outcrops indicate a weak clustering of veins, in agreement with pervasive fluid flow. Fluid channelization, if any, must therefore be looked for at a scale greater than single outcrops and possibly along major tectonic contacts (Herviou & Bonnet, 2023; Jaeckel et al., 2018; Figure 13a); the observed higher vein densities in the studied outcrops might represent zones of more localized deformation and channelized fluid flow that could only be statistically detected on hm- to km-scale transects across the complex. The feasibility of this larger scale approach seems however limited by the characteristic length scale and discontinuity of rock exposures (Figures 2c and 2d). The conclusion that fluid flow was overall pervasive is also consistent with most geochemical studies on the Schistes Lustrés veins, which advocate for local fluid redistribution (e.g., Agard et al., 2000; Cook-Kollars et al., 2014; Epstein et al., 2020; Henry et al., 1996; Herviou et al., 2021; Figures 13a and 13b).

For individual outcrops, 7/12 studied transects (group 1; outcrops #1, 4, 5, 6, 8, 11, 12) have a great proportion of thin veins (D_t in the range 0.92–1.21 with most values greater than 1; see Table 3), a great proportion of small spacings (D_s in the range 1.21–2.48) and a weak clustering of veins (D_c in the range 0.61–0.86 with most values greater than 0.65–0.7). In contrast, 3/12 of the studied transects (group 2; outcrops #3, 9, 10) show a more localized distribution and connection of veins, with a greater proportion of thick veins ($D_t < 1$ and in the range 0.58–0.79), of thick spacings ($D_s < 1$ and in the range 0.72–0.92) and a greater clustering (D_c in the range 0.46–0.63), suggesting a possibly more channelized fluid flow than for group 1. The two remaining transects (group 3; outcrops #2 and 7) show slightly different characteristics, with a greater proportion of thick veins than group 1 ($D_t \sim 0.94$ –0.96), a smaller proportion of thick spacings than group 2 but generally greater than group 1 ($D_s \sim 1.17$ –1.26) and a greater clustering than group 1 ($D_c \sim 0.56$ –0.60). Differences in vein distribution between the various outcrops do not correlate with the abundance of veins in a given outcrop (Figure 4; 10.3%–29.5%, 9.2%–32.4%, 12.1%–22% in groups 1, 2, and 3 respectively; Table 1).

In the slightly more clustered vein systems of groups 2 and 3, 3/5 outcrops belong to the LPM units (outcrops #7, 9, 10) and the mean D_c is similar in both LPM and LPU transects. The combined data sets of LPM outcrops have however a slightly greater proportion of thick veins, thick spacings ($D_t = 0.93$, $D_s = 1.33$) than LPU outcrops ($D_t = 0.97$, $D_s = 1.58$). This could suggest that fluid flow was somewhat more channelized in the LPM outcrops, which could tentatively be ascribed to greater porosity/permeability heterogeneities in the more carbonate-rich LPM protoliths (Herviou et al., 2022). Alternatively, local contrasts in vein spacings and/or vein distribution may essentially reflect strain partitioning, partly along inherited discontinuities (e.g., between the weaker early cleavage or fractures planes), and thereby provide an image of strain distribution.

7.3. Implications for Deformation and Rupture Processes at the Downdip End of the Seismogenic Zone

The studied lawsonite- and Fe-Mg carpholite-bearing crack-seal veins were formed by successive increments of fracturing, fluid infiltration and mineral growth in the same depth/temperature range as deep SST (25–55 km,

350–550°C; Behr & Bürgmann, 2021; Condit et al., 2020; Peacock, 2009). The Schistes Lustrés metasediments contain large amounts of veins (9.2%–32.4% in the studied outcrops; Table 1) and high-pressure hydrous minerals in host rocks (e.g., Lefeuvre et al., 2020), reflecting the ubiquitous presence of fluids at peak burial conditions. Tension gashes filled by high-pressure mineral assemblages and crack-seal textures argue for high fluid pressure during vein formation while the presence of LwsC extension veins oriented at high angles (~80–90°) to the LwsB dilational shear veins implies a low differential stress and a weak shearing potentially caused by high pore fluid pressure (Cox, 2010; Etheridge, 1983; Fagereng et al., 2010). The Schistes Lustrés metasediments may therefore have hosted the low-velocity layer observed in modern subduction zones, downdip of the seismogenic zone (Audet et al., 2009; Bostock, 2013; Calvert et al., 2011; Delph et al., 2021; Hansen et al., 2012), and the rock record of deep SST may be these crack-seal veins as already suggested for such type of dilational shear veins from other complexes (Behr & Bürgmann, 2021; Fagereng et al., 2011; Giuntoli & Viola, 2021, 2022; Kirkpatrick et al., 2021; Ujiie et al., 2018).

Vein distribution suggests that the shear surfaces bounding the elongate LwsB and Fe-Mg carpholite-bearing veins (and some of the LwsC veins; Section 7.1, Figure 12) act as extremely weak planes where preferential slip occurs (Fagereng et al., 2010, 2011; Figures 6a–6e, 12, and 13b). Since we interpret crack-seal spacing as individual slip increments, one may try to compare these data directly with SST data. In LwsB and LwsC veins, the spacings between lawsonite inclusions in trails and fluid inclusion in trails (inclusion bands), are on the order of ~5 μm (Table 3; Section 6.4). These increments are overall smaller than the up to tens of cm-long displacements associated with slow slip events (Behr & Bürgmann, 2021 and references therein) and slightly smaller, yet in a comparable size range, than the individual slip increments estimated for low-frequency earthquakes (0.05–0.12 mm; Bostock et al., 2015; Chestler & Creager, 2017; Thomas et al., 2016). These lawsonite-bearing veins may therefore correspond to the geological record of low-frequency earthquakes, as previously suggested for crack-seal veins of shallower subduction complexes (Fagereng et al., 2011; Tarling et al., 2021; Ujiie et al., 2018; Williams & Kirkpatrick, 2022).

Considering a minimum rupture length L slightly longer than the vein length (~1 m) and up to the outcrop length (~10 m), the calculated shear stress drop $\Delta\tau$, based on slip increments d of ~5 μm and a shear modulus μ of ~3–30 GPa (for sediments; Geist & Bilek, 2001 and references therein), would be in the range 1.5–150 kPa (using $d/L = \Delta\tau/\mu$; Wells & Coppersmith, 1994; see also Fagereng et al., 2011). This value is consistent with shear stress drop estimates for slow-slip events, episodic tremor and slip events and low-frequency earthquakes (1–100 kPa; Behr and Bürgmann and references therein).

The spacings between lawsonite inclusions in trails and inclusion bands are best described by power laws affected by truncation mostly at small spacing values (Section 6.4; Figures 11a–11f). Fault plane geometry, as well as the relationship between the frequency and magnitude of ordinary earthquakes, follow power-law distributions (Gutenberg & Richter, 1954; Jackson & Sanderson, 1992; Pickering et al., 1995, 1996; Watterson, 1986). For SST, while a scaling law distinct from the one of ordinary earthquakes was originally proposed to link their moment and duration (Ide et al., 2007), there is growing evidence that they share similar scaling properties with ordinary earthquakes (Dal Zilio et al., 2020; Gao et al., 2012; Gombert et al., 2016; Michel et al., 2019; Wech et al., 2010). As for ordinary earthquakes, a power-law relationship between magnitude and frequency (Gutenberg-Richter law; Gutenberg & Richter, 1954) was suggested for slow slip events (Chiba, 2019, 2020; Michel et al., 2019; Wech et al., 2010) while the moment-frequency distribution of low-frequency earthquakes was proposed to either follow a power-law (e.g., Bostock et al., 2015) or an exponential distribution (e.g., Chestler & Creager, 2017).

We used the relationship $A = kd^2$ linking the rupture area A , the slip increment d , and the coefficient of proportionality k assumed for circular ruptures (e.g., Dal Zilio et al., 2020). For slip increments of ~5 μm on a 1 m² (vein scale) and 100 m² (outcrop scale) rupture area, the magnitude of k lies between 10¹⁰ and 10¹², respectively. Using these assumptions, the moment magnitude for lawsonite inclusion spacings can be calculated, using $M_w = 2/3 \log(\mu kd^3) - 6.07$ and a shear modulus μ of ~30 GPa. The frequency-magnitude plot reveals a linear trend comparable to the classical Gutenberg-Richter law followed by ordinary earthquakes, slow slip events and potentially low-frequency earthquakes (Figure 13d). It is worth noting that this calculation is a preliminary attempt bearing significant uncertainties: a limited number of samples was used while the b -value of earthquakes generally represent a fault population over time, the spacing distribution is fractal over a small range of values and there are uncertainties whether each crack-seal trail records a full slip increment or not. The obtained

moment magnitudes (-4 to -0.9 and -2.7 to 0.4 for a rupture of 1 and 100 m² respectively; Figure 13d; Figure S5 in Supporting Information S1) are significantly smaller than those of slow slip and episodic tremor and slips events ($M_w \geq 5$; e.g., Behr & Bürgmann, 2021; Michel et al., 2019; Wallace & Beavan, 2010), and somewhat smaller yet closer to those of low-frequency earthquakes ($M_w \geq 0.7$; e.g., Bostock et al., 2015; Chestler & Creager, 2017). These very small moment magnitudes seem consistent with the measured few micrometer-long slip increments, that we relate to inclusion spacings. The fractal exponent (~ 1.3 for 329 spacings and varying between ~ 1.2 and ~ 1.6 depending on the number of spacings considered for the regression; Figure 13d) is similar to the b -value estimated for some slow slip events (b -value range of ~ 0.6 – 1.2 ; Chiba, 2019, 2020; Michel et al., 2019; Wech et al., 2010) and to those of most ordinary subduction earthquakes (b -value generally around 1 ; e.g., Scholz, 2015) but is significantly lower than the b -value obtained for low-frequency earthquakes when a power law distribution is favored (b -value ≥ 5 , at least for the large ones; Bostock et al., 2015; Chestler & Creager, 2017; Figure 13d). Previous works have shown that the b -value of ordinary earthquakes is progressively lower with decreasing magnitudes (e.g., Okal & Romanowicz, 1994; Zhan, 2017) and a similar observation was made for low-frequency earthquakes (Chestler & Creager, 2017). Considering the obtained moment magnitude, slightly lower than those recorded by detected low frequency earthquakes, we argue that the artificial b -value calculated with the inclusion spacing distribution may be consistent with that of small low-frequency earthquakes (Figure 13b).

We therefore tentatively propose that these crack-seal veins formed at the depth of the downdip end of the seismogenic zone may correspond to the record of successive low-frequency earthquakes during subduction of the Liguro-Piemont ocean. The lack of evidence for slow slips in our data would tend to suggest that this type of events did not imprint the rock volumes considered here. This may indicate in turn that slow slip events were localized along larger-scale shear structures, for example, 100 m-long shear bands wrapping around the sections investigated for vein patterns. Highly sheared talcschist horizons found along the contacts between tectonic slices (Herviou & Bonnet, 2023) correspond to potential candidates as the stress amplification observed in talc-bearing rocks has been proposed to record former slow slip events (Hoover et al., 2022).

8. Conclusion

In the Schistes Lustrés metasediments of the Liguro-Piemont domain (Western Alps), abundant lawsonite- and Fe-Mg carpholite-bearing veins formed at blueschist-facies conditions are exposed. This study provides insights about the mechanisms that drive and control vein formation, deformation and fluid flow at the depth range of deep slow slips and tremors nucleation:

- (1) Vein thicknesses fit power-law distributions whereas vein spacings and clustering show significant deviations from power laws, interpreted as the result of truncation artifacts and likely affected by the successive stages of ductile deformation. Vein distribution at the outcrop scale suggests that fluids mostly circulated pervasively through the rock rather than along major localized conduits, in agreement with geochemical studies.
- (2) The study of vein textures at macroscopic and microscopic scale shows that veins were formed by incremental crack-seal mechanisms under tensile and shear failure and possibly between extremely weak planes.
- (3) The spacings between crack-seal inclusion trails and bands, which are in the same order as small slip increments for low-frequency earthquakes, fit a power law for a small fractal range and have fractal exponents similar to those estimated for slow slip events and ordinary subduction earthquakes. Interestingly, the shear stress drop estimated for these crack-seal veins is consistent with those inferred for slow slip events, episodic tremor and slip events and low-frequency earthquakes.
- (4) Taken together, results suggest that the studied veins, formed at the downdip end of the seismogenic zone may represent the record of successive low-frequency earthquakes during subduction of the Liguro-Piemont ocean.

Data Availability Statement

The data used in this manuscript are available in Supporting Information S1 and at (Herviou et al., 2023): <https://doi.org/10.5281/zenodo.8383238>.

Acknowledgments

This study was funded by the BRGM in the frame of the RGF-Alpes project. The authors thank S. Michel for stimulating discussions on scaling laws for slow-slip events. J. Garber is thanked for suggestions on fractals and discussions on the field during the initiation of this work. Å. Fagereng and C. Condit are thanked for their detailed reviews, which helped to significantly improve this manuscript, and I. Manighetti is thanked for the editorial handling. L. Jolivet and H. Raimbourg are thanked for remarks and suggestions. The authors are also grateful to B. Goffé for sharing his enthusiasm on fractals since the 90s.

References

Abers, G. A., MacKenzie, L. S., Rondenay, S., Zhang, Z., Wech, A. G., & Creager, K. C. (2009). Imaging the source region of Cascadia tremor and intermediate-depth earthquakes. *Geology*, 37(12), 1119–1122. <https://doi.org/10.1130/G30143A.1>

Agard, P. (2021). Subduction of oceanic lithosphere in the Alps: Selective and archetypal from (slow-spreading) oceans. *Earth-Science Reviews*, 214, 103517. <https://doi.org/10.1016/j.earscirev.2021.103517>

Agard, P., Goffé, B., Touret, J. L. R., & Vidal, O. (2000). Retrograde mineral and fluid evolution in high-pressure metapelites (Schistes lustrés unit, Western Alps). *Contributions to Mineralogy and Petrology*, 140(3), 296–315. <https://doi.org/10.1007/s004100000190>

Agard, P., & Handy, M. R. (2021). Ocean subduction dynamics in the Alps. *Elements*, 17(1), 9–16. <https://doi.org/10.2138/gselements.17.1.9>

Agard, P., Jolivet, L., & Goffé, B. (2001). Tectonometamorphic evolution of the Schistes Lustrés Complex; implications for the exhumation of HP and UHP rocks in the Western Alps. *Bulletin de la Société Géologique de France*, 172(5), 617–636. <https://doi.org/10.2113/172.5.617>

Agard, P., Monie, P., Jolivet, L., & Goffé, B. (2002). Exhumation of the Schistes Lustrés complex: In situ laser probe ⁴⁰Ar/³⁹Ar constraints and implications for the Western Alps. *Journal of Metamorphic Geology*, 20(6), 599–618. <https://doi.org/10.1046/j.1525-1314.2002.00391.x>

Agard, P., Plunder, A., Angiboust, S., Bonnet, G., & Ruh, J. (2018). The subduction plate interface: Rock record and mechanical coupling (from long to short timescales). *Lithos*, 320–321, 537–566. <https://doi.org/10.1016/j.lithos.2018.09.029>

Agard, P., Yamato, P., Jolivet, L., & Burov, E. (2009). Exhumation of oceanic blueschists and eclogites in subduction zones: Timing and mechanisms. *Earth-Science Reviews*, 92(1–2), 53–79. <https://doi.org/10.1016/j.earscirev.2008.11.002>

Allègre, C. J., Le Mouél, J. L., & Provost, A. (1982). Scaling rules in rock fracture and possible implications for earthquake prediction. *Nature*, 297(5861), 47–49. <https://doi.org/10.1038/297047a0>

André-Mayer, A.-S., & Sausse, J. (2007). Thickness and spatial distribution of veins in a porphyry copper deposit, Rosia Poieni, Romania. *Journal of Structural Geology*, 29(10), 1695–1708. <https://doi.org/10.1016/j.jsg.2007.06.010>

Angiboust, S., & Glodny, J. (2020). Exhumation of eclogitic ophiolitic nappes in the W. Alps: New age data and implications for crustal wedge dynamics. *Lithos*, 356–357, 105374. <https://doi.org/10.1016/j.lithos.2020.105374>

Audet, P., Bostock, M. G., Christensen, N. I., & Peacock, S. M. (2009). Seismic evidence for overpressured subducted oceanic crust and megathrust fault sealing. *Nature*, 457(7225), 76–78. <https://doi.org/10.1038/nature07650>

Audet, P., & Bürgmann, R. (2014). Possible control of subduction zone slow-earthquake periodicity by silica enrichment. *Nature*, 510(7505), 389–392. <https://doi.org/10.1038/nature13391>

Barton, C. A., & Zoback, M. D. (1992). Self-similar distribution and properties of macroscopic fractures at depth in crystalline rock in the Cajon Pass Scientific Drill Hole. *Journal of Geophysical Research*, 97(B4), 5181–5200. <https://doi.org/10.1029/91JB01674>

Barton, C. C. (1995). Fractal analysis of scaling and spatial clustering of fractures. In *Fractals in the Earth sciences* (pp. 141–178). Springer.

Barton, C. C., & Larsen, E. (1985). Fractal geometry of two-dimensional fracture networks at Yucca Mountain, southwest Nevada. *Fundamentals of Rock Joints*. In O. Stephansson (Ed.), *Proceedings of the international symposium on fundamentals of rock joints, Bjorkliden, Lapland, Sweden*.

Bebout, G. E., Agard, P., Kobayashi, K., Moriguti, T., & Nakamura, E. (2013). Devolatilization history and trace element mobility in deeply subducted sedimentary rocks: Evidence from Western Alps HP/UHP suites. *Chemical Geology*, 342, 1–20. <https://doi.org/10.1016/j.chemgeo.2013.01.009>

Behr, W. M., & Bürgmann, R. (2021). What’s down there? The structures, materials and environment of deep-seated slow slip and tremor. *Philosophical Transactions of the Royal Society A*, 379(2193), 20200218. <https://doi.org/10.1098/rsta.2020.0218>

Berger, A., & Bousquet, R. (2008). Subduction-related metamorphism in the Alps: Review of isotopic ages based on petrology and their geodynamic consequences. *Geological Society, London, Special Publications*, 298(1), 117–144. <https://doi.org/10.1144/SP298.7>

Beysac, O., Goffé, B., Chopin, C., & Rouzaud, J. N. (2002). Raman spectra of carbonaceous material in metasediments: A new geothermometer. *Journal of Metamorphic Geology*, 20(9), 859–871. <https://doi.org/10.1046/j.1525-1314.2002.00408.x>

Blenkinsop, T. G. (1991). Cataclasis and processes of particle size reduction. *PAGEOPH*, 136(1), 59–86. <https://doi.org/10.1007/bf00878888>

Blenkinsop, T. G., & Fernandes, T. R. C. (2000). Fractal characterization of particle size distributions in chromitites from the Great Dyke, Zimbabwe. *Pure and Applied Geophysics*, 157(4), 505–521. <https://doi.org/10.1007/p100001104>

Bons, P. D., Elburg, M. A., & Gomez-Rivas, E. (2012). A review of the formation of tectonic veins and their microstructures. *Journal of Structural Geology*, 43, 33–62. <https://doi.org/10.1016/j.jsg.2012.07.005>

Bostock, M. G. (2013). The Moho in subduction zones. *Tectonophysics*, 609, 547–557. <https://doi.org/10.1016/j.tecto.2012.07.007>

Bostock, M. G., Thomas, A. M., Savard, G., Chuang, L., & Rubin, A. M. (2015). Magnitudes and moment-duration scaling of low-frequency earthquakes beneath southern Vancouver Island. *Journal of Geophysical Research: Solid Earth*, 120(9), 6329–6350. <https://doi.org/10.1002/2015JB012195>

Brantley, S. L., Fisher, D. M., Deines, P., Clark, M. B., & Myers, G. (1997). Segregation veins: Evidence for the deformation and dewatering of a low-grade metapelite. In *Deformation-enhanced fluid transport in the Earth’s crust and mantle* (pp. 267–288).

Braun, M. G., & Kelemen, P. B. (2002). Dunite distribution in the Oman Ophiolite: Implications for melt flux through porous dunite conduits. *Geochemistry, Geophysics, Geosystems*, 3(11), 1–21. <https://doi.org/10.1029/2001GC000289>

Brown, J. R., Prejean, S. G., Beroza, G. C., Gombert, J. S., & Haeussler, P. J. (2013). Deep low-frequency earthquakes in tectonic tremor along the Alaska-Aleutian subduction zone. *Journal of Geophysical Research: Solid Earth*, 118(3), 1079–1090. <https://doi.org/10.1029/2012jb009459>

Calvert, A. J., Preston, L. A., & Farahbod, A. M. (2011). Sedimentary underplating at the Cascadia mantle-wedge corner revealed by seismic imaging. *Nature Geoscience*, 4(8), 545–548. <https://doi.org/10.1038/ngeo1195>

Caron, J.-M. (1974). Rapports entre diverses “generations” de lawsonite et les déformations dans les Schistes lustrés des Alpes cottiennes septentrionales (France et Italie). *Bulletin de la Société Géologique de France*, 7, 256–263.

Caron, J. M. (1977). Lithostratigraphie et tectonique des Schistes Lustrés dans les Alpes Cottiennes septentrionales et en Corse orientale. PhD thesis. université de Strasbourg.

Cartwright, I., & Buick, I. S. (2000). Fluid generation, vein formation and the degree of fluid-rock interaction during decompression of high-pressure terranes: The Schistes Lustrés, Alpine Corsica, France. *Journal of Metamorphic Geology*, 18(6), 607–624. <https://doi.org/10.1046/j.1525-1314.2000.00280.x>

Cerchiari, A., Remitti, F., Mittempergher, S., Festa, A., Lugli, F., & Cipriani, A. (2020). Cyclical variations of fluid sources and stress state in a shallow megathrust-zone mélange. *Journal of the Geological Society*, 177(3), 647–659. <https://doi.org/10.1144/jgs2019-072>

Chestler, S. R., & Creager, K. C. (2017). Evidence for a scale-limited low-frequency earthquake source process. *Journal of Geophysical Research: Solid Earth*, 122(4), 3099–3114. <https://doi.org/10.1002/2016JB013717>

Chiba, K. (2019). Spatial and temporal distributions of b-values related to long-term slow-slip and low-frequency earthquakes in the Bungo Channel and Hyuga-nada regions, Japan. *Tectonophysics*, 757, 1–9. <https://doi.org/10.1016/j.tecto.2019.02.021>

- Chiba, K. (2020). Stress state along the western Nankai Trough subduction zone inferred from b-values, long-term slow-slip events, and low-frequency earthquakes. *Earth Planets and Space*, 72(1), 3. <https://doi.org/10.1186/s40623-020-1130-7>
- Clark, M. B., Brantley, S. L., & Fisher, D. M. (1995). Power-law vein-thickness distributions and positive feedback in vein growth. *Geology*, 23(11), 975–978. [https://doi.org/10.1130/0091-7613\(1995\)023<0975:PLVTD>2.3.CO;2](https://doi.org/10.1130/0091-7613(1995)023<0975:PLVTD>2.3.CO;2)
- Condit, C. B., & French, M. E. (2022). Geologic evidence of lithostatic pore fluid pressures at the base of the subduction seismogenic zone. *Geophysical Research Letters*, 49(12), e2022GL098862. <https://doi.org/10.1029/2022gl098862>
- Condit, C. B., Guevara, V. E., Delph, J. R., & French, M. E. (2020). Slab dehydration in warm subduction zones at depths of episodic slip and tremor. *Earth and Planetary Science Letters*, 552, 116601. <https://doi.org/10.1016/j.epsl.2020.116601>
- Cook-Kollars, J., Bebout, G. E., Collins, N. C., Angiboust, S., & Agard, P. (2014). Subduction zone metamorphic pathway for deep carbon cycling: I. Evidence from HP/UHP metasedimentary rocks, Italian Alps. *Chemical Geology*, 386, 31–48. <https://doi.org/10.1016/j.chemgeo.2014.07.013>
- Cox, D. R., & Lewis, P. A. W. (1966). The statistical analysis of series of events.
- Cox, S. F. (1987). Antitaxial crack-seal vein microstructures and their relationship to displacement paths. *Journal of Structural Geology*, 9(7), 779–787. [https://doi.org/10.1016/0191-8141\(87\)90079-4](https://doi.org/10.1016/0191-8141(87)90079-4)
- Cox, S. F. (2010). The application of failure mode diagrams for exploring the roles of fluid pressure and stress states in controlling styles of fracture-controlled permeability enhancement in faults and shear zones. *Geofluids*, 10(1–2), 217–233. <https://doi.org/10.1111/j.1468-8123.2010.00281.x>
- Cubas, N., Agard, P., & Tissandier, R. (2022). Earthquake ruptures and topography of the Chilean margin controlled by plate interface deformation. *Solid Earth*, 13(3), 779–792. <https://doi.org/10.5194/se-13-779-2022>
- Dal Zilio, L., Lapusta, N., & Avouac, J. (2020). Unraveling scaling properties of slow-slip events. *Geophysical Research Letters*, 47(10), e2020GL087477. <https://doi.org/10.1029/2020GL087477>
- Delph, J. R., Levander, A., & Niu, F. (2018). Fluid controls on the heterogeneous seismic characteristics of the Cascadia margin. *Geophysical Research Letters*, 45(20), 11021–11029. <https://doi.org/10.1029/2018GL079518>
- Delph, J. R., Thomas, A. M., & Levander, A. (2021). Subcretionary tectonics: Linking variability in the expression of subduction along the Cascadia forearc. *Earth and Planetary Science Letters*, 556, 116724. <https://doi.org/10.1016/j.epsl.2020.116724>
- Deville, E., Fudral, S., Lagabriele, Y., Marthaler, M., & Sartori, M. (1992). From oceanic closure to continental collision: A synthesis of the “Schistes lustrés” metamorphic complex of the Western Alps. *Geological Society of America Bulletin*, 104(2), 127–139. [https://doi.org/10.1130/0016-7606\(1992\)104<0127:foctcc>2.3.co;2](https://doi.org/10.1130/0016-7606(1992)104<0127:foctcc>2.3.co;2)
- Dragert, H., Wang, K., & James, T. S. (2001). A silent slip event on the deeper Cascadia subduction interface. *Science*, 292(5521), 1525–1528. <https://doi.org/10.1126/science.1060152>
- Epstein, G. S., Bebout, G. E., Angiboust, S., & Agard, P. (2020). Scales of fluid-rock interaction and carbon mobility in the deeply underplated and HP-Metamorphosed Schistes Lustrés, Western Alps. *Lithos*, 354–355, 105229. <https://doi.org/10.1016/j.lithos.2019.105229>
- Etheridge, M. A. (1983). Differential stress magnitudes during regional deformation and metamorphism: Upper bound imposed by tensile fracturing. *Geology*, 11(4), 31–234. [https://doi.org/10.1130/0091-7613\(1983\)11<231:dsmdrd>2.0.co;2](https://doi.org/10.1130/0091-7613(1983)11<231:dsmdrd>2.0.co;2)
- Fagereng, Å. (2011). Fractal vein distributions within a fault-fracture mesh in an exhumed accretionary mélange, Chrystalls Beach Complex, New Zealand. *Journal of Structural Geology*, 33(5), 918–927. <https://doi.org/10.1016/j.jsg.2011.02.009>
- Fagereng, Å., & Cooper, A. F. (2010). The metamorphic history of rocks buried, accreted and exhumed in an accretionary prism: An example from the Otago Schist, New Zealand. *Journal of Metamorphic Geology*, 28(9), 935–954. <https://doi.org/10.1111/j.1525-1314.2010.00900.x>
- Fagereng, Å., & Harris, C. (2014). Interplay between fluid flow and fault–fracture mesh generation within underthrust sediments: Geochemical evidence from the Chrystalls Beach Complex, New Zealand. *Tectonophysics*, 612, 147–157. <https://doi.org/10.1016/j.tecto.2013.12.002>
- Fagereng, Å., Remitti, F., & Sibson, R. H. (2010). Shear veins observed within anisotropic fabric at high angles to the maximum compressive stress. *Nature Geoscience*, 3(7), 482–485. <https://doi.org/10.1038/ngeo898>
- Fagereng, Å., Remitti, F., & Sibson, R. H. (2011). Incrementally developed slickenfibers—Geological record of repeating low stress-drop seismic events? *Tectonophysics*, 510(3–4), 381–386. <https://doi.org/10.1016/j.tecto.2011.08.015>
- Fisher, D. M., & Brantley, S. L. (1992). Models of quartz overgrowth and vein formation: Deformation and episodic fluid flow in an ancient subduction zone. *Journal of Geophysical Research*, 97(B13), 20043–20061. <https://doi.org/10.1029/92JB01582>
- Fisher, D. M., & Brantley, S. L. (2014). The role of silica redistribution in the evolution of slip instabilities along subduction interfaces: Constraints from the Kodiak accretionary complex, Alaska. *Journal of Structural Geology*, 69, 395–414. <https://doi.org/10.1016/j.jsg.2014.03.010>
- Fisher, D. M., Brantley, S. L., Everett, M., & Dzvoni, J. (1995). Cyclic fluid flow through a regionally extensive fracture network within the Kodiak accretionary prism. *Journal of Geophysical Research*, 100(B7), 12881–12894. <https://doi.org/10.1029/94JB02816>
- Foxford, K. A., Nicholson, R., Polya, D. A., & Hebblethwaite, R. P. B. (2000). Extensional failure and hydraulic valving at Minas da Panasqueira, Portugal: Evidence from vein spatial distributions, displacements and geometries. *Journal of Structural Geology*, 22(8), 1065–1086. [https://doi.org/10.1016/S0191-8141\(00\)00029-8](https://doi.org/10.1016/S0191-8141(00)00029-8)
- Fudral, S. (1996). Etude géologique de la suture tethysienne dans les Alpes franco-italiennes Nord-Occidentales de la Doire Ripaire (Italie) à la région de Bourg Saint-Maurice. PhD thesis. Université de Savoie.
- Gabalda, S., Beyssac, O., Jolivet, L., Agard, P., & Chopin, C. (2009). Thermal structure of a fossil subduction wedge in the Western Alps. *Terra Nova*, 21(1), 28–34. <https://doi.org/10.1111/j.1365-3121.2008.00849.x>
- Ganzhorn, A. C., Pilorgé, H., & Reynard, B. (2019). Porosity of metamorphic rocks and fluid migration within subduction interfaces. *Earth and Planetary Science Letters*, 522, 107–117. <https://doi.org/10.1016/j.epsl.2019.06.030>
- Gao, H., Schmidt, D. A., & Weldon, R. J. (2012). Scaling relationships of source parameters for slow slip events. *Bulletin of the Seismological Society of America*, 102(1), 352–360. <https://doi.org/10.1785/0120110096>
- Geist, E. L., & Bilek, S. L. (2001). Effect of depth-dependent shear modulus on tsunami generation along subduction zones. *Geophysical Research Letters*, 28(7), 1315–1318. <https://doi.org/10.1029/2000gl012385>
- Gillespie, P. A., Howard, C. B., Walsh, J. J., & Watterson, J. (1993). Measurement and characterisation of spatial distributions of fractures. *Tectonophysics*, 226(1–4), 113–141. [https://doi.org/10.1016/0040-1951\(93\)90114-y](https://doi.org/10.1016/0040-1951(93)90114-y)
- Gillespie, P. A., Johnston, J. D., Loriga, M. A., McCaffrey, K. J. W., Walsh, J. J., & Watterson, J. (1999). Influence of layering on vein systematics in line samples. *Geological Society, London, Special Publications*, 155(1), 35–56. <https://doi.org/10.1144/GSL.SP.1999.155.01.05>
- Giuntoli, F., & Viola, G. (2021). Cyclic brittle-ductile oscillations recorded in exhumed high-pressure continental units: A record of deep episodic tremor and slow slip events in the Northern Apennines. *Geochemistry, Geophysics, Geosystems*, 22(9), e2021GC009805. <https://doi.org/10.1029/2021GC009805>
- Giuntoli, F., & Viola, G. (2022). A likely geological record of deep tremor and slow slip events from a subducted continental broken formation. *Scientific Reports*, 12, 1–14. <https://doi.org/10.1038/s41598-022-08489-2>

- Goffé, B., & Chopin, C. (1986). High-pressure metamorphism in the Western Alps: Zoneography of metapelites, chronology and consequences. *Schweizerische Mineralogische Und Petrographische Mitteilungen*, 66, 41–52. <https://doi.org/10.5169/SEALS-50880>
- Gomberg, J., Wech, A., Creager, K., Obara, K., & Agnew, D. (2016). Reconsidering earthquake scaling. *Geophysical Research Letters*, 43(12), 6243–6251. <https://doi.org/10.1002/2016GL069967>
- Gratier, J. P., Dysthe, D. K., & Renard, F. (2013). The role of pressure solution creep in the ductility of the Earth's upper crust. *Advances in Geophysics*, 54, 47–179.
- Gutenberg, B., & Richter, C. F. (1954). *Seismicity of the Earth*. Princeton University Press.
- Gyomlai, T., Agard, P., Herviou, C., Jolivet, L., Monié, P., Mendes, K., & Iemmolo, A. (2023). In situ Rb–Sr and ⁴⁰Ar–³⁹Ar dating of distinct mica generations in the exhumed subduction complex of the Western Alps. *Contributions to Mineralogy and Petrology*, 178(9), 58. <https://doi.org/10.1007/s00410-023-02042-8>
- Hansen, R. T. J., Bostock, M. G., & Christensen, N. I. (2012). Nature of the low velocity zone in Cascadia from receiver function waveform inversion. *Earth and Planetary Science Letters*, 337(338), 25–38. <https://doi.org/10.1016/j.epsl.2012.05.031>
- Henry, C., Burkhard, M., & Goffé, B. (1996). Evolution of synmetamorphic veins and their wallrocks through a Western Alps transect: No evidence for large-scale fluid flow. Stable isotope, major- and trace-element systematics. *Chemical Geology*, 127(1–3), 81–109. [https://doi.org/10.1016/0009-2541\(95\)00106-9](https://doi.org/10.1016/0009-2541(95)00106-9)
- Herviou, C., Agard, P., Plunder, A., Mendes, K., Verlaquet, A., Deldicque, D., & Cubas, N. (2022). Subducted fragments of the Liguro-Piemont ocean, Western Alps: Spatial correlations and offscraping mechanisms during subduction. *Tectonophysics*, 229267, 229267. <https://doi.org/10.1016/j.tecto.2022.229267>
- Herviou, C., Agard, P., Verlaquet, A., Gyomlai, T., Bonnet, G., Mendes, K., & Plunder, A. (2023). Supporting data for Fractal distribution of subduction-related crack-seal veins (Schistes Lustrés, W. Alps): Implications for fluid flow and rupture processes at the downdip end of the seismogenic zone [Dataset]. Zenodo. <https://doi.org/10.5281/zenodo.8383238>
- Herviou, C., & Bonnet, G. (2023). Paleocene-Eocene high-pressure carbonation of Western Alps serpentinites: Positive feedback between deformation and CO₂-CH₄ fluid ingress responsible for slab slicing? *Geochemistry, Geophysics, Geosystems*, 24(3), e2022GC010557. <https://doi.org/10.1029/2022gc010557>
- Herviou, C., Verlaquet, A., Agard, P., Locatelli, M., Raimbourg, H., Lefeuvre, B., & Dubacq, B. (2021). Along-dip variations of subduction fluids: The 30–80 km depth traverse of the Schistes Lustrés complex (Queyras-Monviso, W. Alps). *Lithos*, 394–395, 106168. <https://doi.org/10.1016/j.lithos.2021.106168>
- Holland, M., & Urai, J. L. (2010). Evolution of anastomosing crack–seal vein networks in limestones: Insight from an exhumed high-pressure cell, Jabal Shams, Oman Mountains. *Journal of Structural Geology*, 32(9), 1279–1290. <https://doi.org/10.1016/j.jsg.2009.04.011>
- Hooker, J. N., Laubach, S. E., & Marrett, R. (2013). Fracture-aperture size—Frequency, spatial distribution, and growth processes in strata-bounded and non-strata-bounded fractures, Cambrian Mesón Group, NW Argentina. *Journal of Structural Geology*, 54, 54–71. <https://doi.org/10.1016/j.jsg.2013.06.011>
- Hoover, W. F., Condit, C. B., Lindquist, P. C., Moser, A. C., & Guevara, V. E. (2022). Episodic slow slip hosted by talc-bearing metasomatic rocks: High strain rates and stress amplification in a chemically reacting shear zone. *Geophysical Research Letters*, 49(21), e2022GL101083. <https://doi.org/10.1029/2022gl101083>
- Hoover, W. F., Penniston-Dorland, S., Piccoli, P., & Kylander-Clark, A. (2023). Reaction-induced porosity in an eclogite-facies vein selvage (Monviso Ophiolite, W. Alps): Textural evidence and in situ trace elements and Sr isotopes in apatite. *Journal of Petrology*, 64(1), egac128. <https://doi.org/10.1093/petrology/egac128>
- Ide, S., Beroza, G. C., Shelly, D. R., & Uchide, T. (2007). A scaling law for slow earthquakes. *Nature*, 447(7140), 76–79. <https://doi.org/10.1038/nature05780>
- Jackson, P., & Sanderson, D. J. (1992). Scaling of fault displacements from the Badajoz-Cordoba shear zone, SW Spain. *Tectonophysics*, 210(3–4), 189–190. [https://doi.org/10.1016/0040-1951\(92\)90321-v](https://doi.org/10.1016/0040-1951(92)90321-v)
- Jaekel, K., Bebout, G. E., & Angiboust, S. (2018). Deformation-enhanced fluid and mass transfer along Western and Central Alps paleo-subduction interfaces: Significance for carbon cycling models. *Geosphere*, 14(6), 2355–2375. <https://doi.org/10.1130/GES01587.1>
- Johnston, J. D., & McCaffrey, K. J. W. (1996). Fractal geometries of vein systems and the variation of scaling relationships with mechanism. *Journal of Structural Geology*, 18(2–3), 349–358. [https://doi.org/10.1016/S0191-8141\(96\)80055-1](https://doi.org/10.1016/S0191-8141(96)80055-1)
- Kirkpatrick, J. D., Fagereng, Å., & Shelly, D. R. (2021). Geological constraints on the mechanisms of slow earthquakes. *Nature Reviews Earth & Environment*, 2(4), 285–301. <https://doi.org/10.1038/s43017-021-00148-w>
- Lagabriele, Y. (1987). Les ophiolites: Marqueurs de l'histoire tectonique des domaines océaniques. PhD thesis.
- Lagabriele, Y., & Cannat, M. (1990). Alpine Jurassic ophiolites resemble the modern central Atlantic basement. *Geology*, 18(4), 319–322. [https://doi.org/10.1130/0091-7613\(1990\)018<0319:ajortm>2.3.co;2](https://doi.org/10.1130/0091-7613(1990)018<0319:ajortm>2.3.co;2)
- Lahiri, S., Rana, V., Bhatt, S., & Mamtani, M. A. (2020). Paleostress and statistical analysis using quartz veins from mineralized and non-mineralized zones: Application for exploration targeting. *Journal of Structural Geology*, 133, 104006. <https://doi.org/10.1016/j.jsg.2020.104006>
- La Pointe, P. R. (1988). A method to characterize fracture density and connectivity through fractal geometry. *International Journal of Rock Mechanics and Mining Sciences & Geomechanics Abstracts*, 25(6), 421–429. [https://doi.org/10.1016/0148-9062\(88\)90982-5](https://doi.org/10.1016/0148-9062(88)90982-5)
- Lay, T., Kanamori, H., Ammon, C. J., Koper, K. D., Hutko, A. R., Ye, L., et al. (2012). Depth-varying rupture properties of subduction zone megathrust faults. *Journal of Geophysical Research*, 117(B4), B04311. <https://doi.org/10.1029/2011JB009133>
- Ledéser, B., Dubois, J., Genter, A., & Meunier, A. (1993). Fractal analysis of fractures applied to Soultz-sous-Forets hot dry rock geothermal program. *Journal of Volcanology and Geothermal Research*, 57(1–2), 1–17. [https://doi.org/10.1016/0377-0273\(93\)90028-P](https://doi.org/10.1016/0377-0273(93)90028-P)
- Lefeuvre, B., Agard, P., Verlaquet, A., Dubacq, B., & Plunder, A. (2020). Massive formation of lawsonite in subducted sediments from the Schistes Lustrés (W. Alps): Implications for mass transfer and decarbonation in cold subduction zones. *Lithos*, 370–371, 105629. <https://doi.org/10.1016/j.lithos.2020.105629>
- Lemonnier, N., Homberg, C., Roche, V., Rocher, M., Boullier, A., & Schnyder, J. (2020). Microstructures of bedding-parallel faults under multistage deformation: Examples from the Southeast Basin of France. *Journal of Structural Geology*, 140, 104138. <https://doi.org/10.1016/j.jsg.2020.104138>
- Locatelli, M., Verlaquet, A., Agard, P., Pettke, T., & Federico, L. (2019). Fluid pulses during stepwise brecciation at intermediate subduction depths (Monviso Eclogites, W. Alps): First internally then externally sourced. *Geochemistry, Geophysics, Geosystems*, 20(11), 5285–5318. <https://doi.org/10.1029/2019GC008549>
- Magde, L. S., Dick, H. J. B., & Hart, S. R. (1995). Tectonics, alteration and the fractal distribution of hydrothermal veins in the lower ocean crust. *Earth and Planetary Science Letters*, 129(1–4), 103–119. [https://doi.org/10.1016/0012-821X\(94\)00239-U](https://doi.org/10.1016/0012-821X(94)00239-U)
- Mandelbrot, B. B. (1982). *The fractal geometry of nature* (Vol. 1). WH Freeman.

- Manning, C. E. (1994). Fractal clustering of metamorphic veins. *Geology*, 22(4), 335–338. [https://doi.org/10.1130/0091-7613\(1994\)022<0335:FCOMV>2.3.CO;2](https://doi.org/10.1130/0091-7613(1994)022<0335:FCOMV>2.3.CO;2)
- Mazzarini, F., Musumeci, G., & Cruden, A. R. (2011). Vein development during folding in the upper brittle crust: The case of tourmaline-rich veins of eastern Elba Island, northern Tyrrhenian Sea, Italy. *Journal of Structural Geology*, 33(10), 1509–1522. <https://doi.org/10.1016/j.jsg.2011.07.001>
- McCaffrey, K., Johnson, J. D., & Feely, M. (1993). Use of fractal statistics in the analysis of Mo-Cu mineralisation at Mace Head, County Galway. *Irish Journal of Earth Sciences*, 1, 139–148.
- McCaffrey, K. J. W., & Johnston, J. D. (1996). Fractal analysis of a mineralised vein deposit: Curraghinalt gold deposit, County Tyrone. *Mineralium Deposita*, 31(1–2), 52–58. <https://doi.org/10.1007/bf00225395>
- Michel, S., Gualandi, A., & Avouac, J.-P. (2019). Similar scaling laws for earthquakes and Cascadia slow-slip events. *Nature*, 574(7779), 522–526. <https://doi.org/10.1038/s41586-019-1673-6>
- Monecke, T., Gemmel, J. B., & Monecke, J. (2001). Fractal distributions of veins in drill core from the Hellyer VHMS deposit, Australia: Constraints on the origin and evolution of the mineralising system. *Mineralium Deposita*, 36(5), 406–415. <https://doi.org/10.1007/s001260100161>
- Muñoz-Montecinos, J., Angiboust, S., Cambeses, A., & García-Casco, A. (2020). Multiple veining in a paleo-accretionary wedge: The metamorphic rock record of prograde dehydration and transient high pore-fluid pressures along the subduction interface (Western Series, central Chile). *Geosphere*, 16(3), 765–786. <https://doi.org/10.1130/GES0227.1>
- Muñoz-Montecinos, J., Angiboust, S., García-Casco, A., Glodny, J., & Bebout, G. (2021). Episodic hydrofracturing and large-scale flushing along deep subduction interfaces: Implications for fluid transfer and carbon recycling (Zagros Orogen, southeastern Iran). *Chemical Geology*, 571, 120173. <https://doi.org/10.1016/j.chemgeo.2021.120173>
- Muñoz-Montecinos, J., Angiboust, S., García-Casco, A., & Raimondo, T. (2023). Shattered veins elucidate brittle creep processes in the deep slow slip and tremor region. *Tectonics*, 42(4), 2022TC007605. <https://doi.org/10.1029/2022tc007605>
- Narr, W., & Suppe, J. (1991). Joint spacing in sedimentary rocks. *Journal of Structural Geology*, 13(9), 1037–1048. [https://doi.org/10.1016/0191-8141\(91\)90055-n](https://doi.org/10.1016/0191-8141(91)90055-n)
- Nishiyama, N., Ujiie, K., & Kano, M. (2021). Spatial changes in inclusion band spacing as an indicator of temporal changes in slow slip and tremor recurrence intervals. *Earth Planets and Space*, 73(1), 126. <https://doi.org/10.1186/s40623-021-01448-7>
- Obara, K. (2002). Nonvolcanic deep tremor associated with subduction in southwest Japan. *Science*, 296(5573), 1679–1681. <https://doi.org/10.1126/science.1070378>
- Obara, K., & Kato, A. (2016). Connecting slow earthquakes to huge earthquakes. *Science*, 353(6296), 253–257. <https://doi.org/10.1126/science.aaf1512>
- Okal, E. A., & Romanowicz, B. A. (1994). On the variation of b-values with earthquake size. *Physics of the Earth and Planetary Interiors*, 87(1–2), 55–76. [https://doi.org/10.1016/0031-9201\(94\)90021-3](https://doi.org/10.1016/0031-9201(94)90021-3)
- Oliver, N. H. S., & Bons, P. D. (2001). Mechanisms of fluid flow and fluid-rock interaction in fossil metamorphic hydrothermal systems inferred from vein-wallrock patterns, geometry and microstructure. *Geofluids*, 1(2), 137–162. <https://doi.org/10.1046/j.1468-8123.2001.00013.x>
- Oncken, O., Angiboust, S., & Dresen, G. (2021). Slow slip in subduction zones: Reconciling deformation fabrics with instrumental observations and laboratory results. *Geosphere*, 18(1), 104–129. <https://doi.org/10.1130/GES02382.1>
- Ortega, O. J., Marrett, R. A., & Laubach, S. E. (2006). A scale-independent approach to fracture intensity and average spacing measurement. *AAPG Bulletin*, 90(2), 193–208. <https://doi.org/10.1306/08250505059>
- Palazzin, G., Raimbourg, H., Famin, V., Jolivet, L., Kusaba, Y., & Yamaguchi, A. (2016). Deformation processes at the down-dip limit of the seismogenic zone: The example of Shimanto accretionary complex. *Tectonophysics*, 687, 28–43. <https://doi.org/10.1016/j.tecto.2016.08.013>
- Paulatto, M., Laïgle, M., Galve, A., Charvis, P., Sapin, M., Bayrakci, G., et al. (2017). Dehydration of subducting slow-spread oceanic lithosphere in the Lesser Antilles. *Nature Communications*, 8(1), 15980. <https://doi.org/10.1038/ncomms15980>
- Peacock, S. M. (2009). Thermal and metamorphic environment of subduction zone episodic tremor and slip. *Journal of Geophysical Research*, 114, B00A07. <https://doi.org/10.1029/2008jb005978>
- Peacock, S. M., Christensen, N. I., Bostock, M. G., & Audet, P. (2011). High pore pressures and porosity at 35 km depth in the Cascadia subduction zone. *Geology*, 39(5), 471–474. <https://doi.org/10.1130/G31649.1>
- Peacock, S. M., & Hyndman, R. D. (1999). Hydrous minerals in the mantle wedge and the maximum depth of subduction thrust earthquakes. *Geophysical Research Letters*, 26(16), 2517–2520. <https://doi.org/10.1029/1999GL900558>
- Pickering, G., Bull, J. M., & Sanderson, D. J. (1995). Sampling power-law distributions. *Tectonophysics*, 248(1–2), 1–20. [https://doi.org/10.1016/0040-1951\(95\)00030-q](https://doi.org/10.1016/0040-1951(95)00030-q)
- Pickering, G., Bull, J. M., & Sanderson, D. J. (1996). Scaling of fault displacements and implications for the estimation of sub-seismic strain. *Geological Society, London, Special Publications*, 99(1), 11–26. <https://doi.org/10.1144/GSL.SP.1996.099.01.03>
- Plunder, A., Agard, P., Chopin, C., Pourteau, A., & Okay, A. I. (2015). Accretion, underplating and exhumation along a subduction interface: From subduction initiation to continental subduction (Tavşanlı zone, W. Turkey). *Lithos*, 226, 233–254. <https://doi.org/10.1016/j.lithos.2015.01.007>
- Plunder, A., Agard, P., Dubacq, B., Chopin, C., & Bellanger, M. (2012). How continuous and precise is the record of P-T paths? Insights from combined thermobarometry and thermodynamic modelling into subduction dynamics (Schistes Lustrés, W. Alps). *Journal of Metamorphic Geology*, 30(3), 323–346. <https://doi.org/10.1111/j.1525-1314.2011.00969.x>
- Raimbourg, H., Famin, V., Palazzin, G., Mayoux, M., Jolivet, L., Ramboz, C., & Yamaguchi, A. (2018). Fluid properties and dynamics along the seismogenic plate interface. *Geosphere*, 14(2), 469–491. <https://doi.org/10.1130/GES01504.1>
- Raimbourg, H., Rajič, K., Moris-Muttoni, B., Famin, V., Palazzin, G., Fisher, D., et al. (2021). Quartz vein geochemistry records deformation processes in convergent zones. *Geochemistry, Geophysics, Geosystems*, 22(4), e2020GC009201. <https://doi.org/10.1029/2020GC009201>
- Rajič, K., Raimbourg, H., Lerouge, C., Famin, V., Dubacq, B., Canizarés, A., et al. (2023). Metamorphic reactions and their implication for the fluid budget in metapelites at seismogenic depths in subduction zones. *Tectonophysics*, 857, 229844. <https://doi.org/10.1016/j.tecto.2023.229844>
- Ramsay, J. G. (1980). The crack-seal mechanism of rock deformation. *Nature*, 284(5752), 135–139. <https://doi.org/10.1038/284135a0>
- Renard, F., Andréani, M., Boullier, A.-M., & Labaume, P. (2005). Crack-seal patterns: Records of uncorrelated stress release variations in crustal rocks. *Geological Society, London, Special Publications*, 243(1), 67–79. <https://doi.org/10.1144/GSL.SP.2005.243.01.07>
- Roberts, S., Sanderson, D. J., & Gumiel, P. (1999). Fractal analysis and percolation properties of veins. *Geological Society, London, Special Publications*, 155(1), 7–16. <https://doi.org/10.1144/GSL.SP.1999.155.01.03>
- Roedder, E. (1984). Volume 12: Fluid inclusions. *Reviews in Mineralogy*, 12.
- Rogers, G., & Dragert, H. (2003). Episodic tremor and slip on the Cascadia subduction zone: The chatter of silent slip. *Science*, 300(5627), 1942–1943. <https://doi.org/10.1126/science.1084783>

- Saffer, D. M., & Tobin, H. J. (2011). Hydrogeology and mechanics of subduction zone forearcs: Fluid flow and pore pressure. *Annual Review of Earth and Planetary Sciences*, 39(1), 157–186. <https://doi.org/10.1146/annurev-earth-040610-133408>
- Sanderson, D. J., Roberts, S., & Gumiel, P. (1994). A fractal relationship between vein thickness and gold grade in drill core from La Codosera, Spain. *Economic Geology*, 89(1), 168–173. <https://doi.org/10.2113/gsecongeo.89.1.168>
- Sanderson, D. J., Roberts, S., Gumiel, P., & Greenfield, C. (2008). Quantitative analysis of Tin- and Tungsten-bearing sheeted vein systems. *Economic Geology*, 103(5), 1043–1056. <https://doi.org/10.2113/gsecongeo.103.5.1043>
- Schmidt, M. W., & Poli, S. (2014). Devolatilization during subduction. In *Treatise on geochemistry* (pp. 669–701). Elsevier. <https://doi.org/10.1016/B978-0-08-095975-7.00321-1>
- Scholz, C. H. (2015). On the stress dependence of the earthquake b value. *Geophysical Research Letters*, 42(5), 1399–1402. <https://doi.org/10.1002/2014GL062863>
- Schwartz, S., Gautheron, C., Ketcham, R. A., Brunet, F., Corre, M., Agranian, A., et al. (2020). Unraveling the exhumation history of high-pressure ophiolites using magnetite (U-Th-Sm)/He thermochronometry. *Earth and Planetary Science Letters*, 543, 116359. <https://doi.org/10.1016/j.epsl.2020.116359>
- Schwartz, S., Guillot, S., Reynard, B., Lafay, R., Debret, B., Nicollet, C., et al. (2013). Pressure–temperature estimates of the lizardite/antigorite transition in high pressure serpentinites. *Lithos*, 178, 197–210. <https://doi.org/10.1016/j.lithos.2012.11.023>
- Schwartz, S., Lardeaux, J. M., Tricart, P., Guillot, S., & Labrin, E. (2007). Diachronous exhumation of HP-LT metamorphic rocks from south-western Alps: Evidence from fission-track analysis. *Terra Nova*, 19(2), 133–140. <https://doi.org/10.1111/j.1365-3121.2006.00728.x>
- Simpson, G. D. H. (2000). Synmetamorphic vein spacing distributions: Characterisation and origin of a distribution of veins from NW Sardinia, Italy. *Journal of Structural Geology*, 22(3), 335–348. [https://doi.org/10.1016/S0191-8141\(99\)00161-3](https://doi.org/10.1016/S0191-8141(99)00161-3)
- Spandler, C., Pettko, T., & Rubatto, D. (2011). Internal and external fluid sources for eclogite-facies veins in the Monviso meta-ophiolite, Western Alps: Implications for fluid flow in subduction zones. *Journal of Petrology*, 52(6), 1207–1236. <https://doi.org/10.1093/petrology/egr025>
- Spandler, C., & Pirard, C. (2013). Element recycling from subducting slabs to arc crust: A review. *Lithos*, 170–171, 208–223. <https://doi.org/10.1016/j.lithos.2013.02.016>
- Stowell, J. F. W., Watson, A. P., & Hudson, N. F. C. (1999). Geometry and population systematics of a quartz vein set, Holy Island, Anglesey, North Wales. *Geological Society, London, Special Publications*, 155(1), 17–33. <https://doi.org/10.1144/GSL.SP.1999.155.01.04>
- Tarling, M. S., Smith, S. A., Rooney, J. S., Viti, C., & Gordon, K. C. (2021). A common type of mineralogical banding in serpentine crack-seal veins. *Earth and Planetary Science Letters*, 564, 116930. <https://doi.org/10.1016/j.epsl.2021.116930>
- Tewksbury-Christle, C. M., & Behr, W. M. (2021). Constraints from exhumed rocks on the seismic signature of the deep subduction interface. *Geophysical Research Letters*, 48(18), e2021GL093831. <https://doi.org/10.1029/2021GL093831>
- Thomas, A. M., Beroza, G. C., & Shelly, D. R. (2016). Constraints on the source parameters of low-frequency earthquakes on the San Andreas Fault. *Geophysical Research Letters*, 43(4), 1464–1471. <https://doi.org/10.1002/2015gl067173>
- Toriumi, A., & Teruya, J. (1988). Tectono-metamorphism of the Shimanto Belt. *Modern Geology*, 12, 303–324.
- Tricart, P., & Schwartz, S. (2006). A north-south section across the Queyras Schistes lustrés (Piedmont zone, Western Alps): Syn-collision reformation of a subduction wedge. *Eclogae Geologicae Helveticae*, 99(3), 429–442. <https://doi.org/10.1007/s00015-006-1197-6>
- Turcotte, D. L. (1986). Fractals and fragmentation. *Journal of Geophysical Research*, 91(B2), 1921–1926. <https://doi.org/10.1029/JB091iB02p01921>
- Turcotte, D. L. (1989). Fractals in geology and geophysics. *PAGEOPH*, 131(1–2), 26–196. <https://doi.org/10.1007/bf00874486>
- Ujii, K., Saishu, H., Fagereng, A., Nishiyama, N., Otsubo, M., Masuyama, H., & Kagi, H. (2018). An explanation of episodic tremor and slow slip constrained by crack-seal veins and viscous shear in subduction mélange. *Geophysical Research Letters*, 45(11), 5371–5379. <https://doi.org/10.1029/2018GL078374>
- Valley, J. W. (1986). Stable isotope geochemistry of metamorphic rocks. 445–490. Stable isotopes in high temperature geological processes.
- Vannucchi, P., Remitti, F., Bettelli, G., Boschi, C., & Dallai, L. (2010). Fluid history related to the early Eocene-middle Miocene convergent system of the Northern Apennines (Italy): Constraints from structural and isotopic studies. *Journal of Geophysical Research*, 115(B5), B05405. <https://doi.org/10.1029/2009JB006590>
- Velde, B., Dubois, J., Moore, D., & Touchard, G. (1991). Fractal patterns of fractures in granites. *Earth and Planetary Science Letters*, 104(1), 25–35. [https://doi.org/10.1016/0012-821x\(91\)90234-9](https://doi.org/10.1016/0012-821x(91)90234-9)
- Velde, B., Dubois, J., Touchard, G., & Badri, A. (1990). Fractal analysis of fractures in rocks: The Cantor's Dust method. *Tectonophysics*, 179(3–4), 345–352. [https://doi.org/10.1016/0040-1951\(90\)90300-w](https://doi.org/10.1016/0040-1951(90)90300-w)
- Verlaguet, A., Goffé, B., Brunet, F., Poinssot, C., Vidal, O., Findling, N., & Menut, D. (2011). Metamorphic veining and mass transfer in a chemically closed system: A case study in Alpine metabasites (western Vanoise). *Journal of Metamorphic Geology*, 29(3), 275–300. <https://doi.org/10.1111/j.1525-1314.2010.00918.x>
- Wallace, L. M., & Beavan, J. (2010). Diverse slow slip behavior at the Hikurangi subduction margin, New Zealand. *Journal of Geophysical Research*, 115(B12), B12402. <https://doi.org/10.1029/2010jb007717>
- Watterson, J. (1986). Fault dimensions, displacements and growth. *Pure and Applied Geophysics*, 124(1–2), 365–373. <https://doi.org/10.1007/bf00875732>
- Wech, A. G., Creager, K. C., Houston, H., & Vidale, J. E. (2010). An earthquake-like magnitude-frequency distribution of slow slip in northern Cascadia. *Geophysical Research Letters*, 37(22), L22310. <https://doi.org/10.1029/2010GL044881>
- Wells, D. L., & Coppersmith, K. J. (1994). New empirical relationships among magnitude, rupture length, rupture width, rupture area, and surface displacement. *Bulletin of the Seismological Society of America*, 84, 974–1002.
- Widmer, T., & Thompson, A. B. (2001). Local origin of high pressure vein material in eclogite facies rocks of the Zermatt-Saas-Zone, Switzerland. *American Journal of Science*, 301(7), 627–656. <https://doi.org/10.2475/ajs.301.7.627>
- Williams, R. T., & Kirkpatrick, J. D. (2022). Are low-frequency earthquake moments area- or slip-limited? A rock record examination. *Geophysical Research Letters*, 49(2), 2021GL095759. <https://doi.org/10.1029/2021gl095759>
- Yarushina, V. M., & Podladchikov, Y. Y. (2015). (De) compaction of porous viscoelastoplastic media: Model formulation. *Journal of Geophysical Research: Solid Earth*, 120(6), 4146–4170. <https://doi.org/10.1002/2014jb011258>
- Zhan, Z. (2017). Gutenberg–Richter law for deep earthquakes revisited: A dual-mechanism hypothesis. *Earth and Planetary Science Letters*, 461, 1–7. <https://doi.org/10.1016/j.epsl.2016.12.030>